MOX-Report No. 29/2015

Review of Discontinuous Galerkin Finite Element Methods for Partial Differential Equations on Complicated Domains

Antonietti, P.F.; Cangiani, A.; Collis, J.; Dong, Z.; Georgoulis, E.H.; Giani, S.; Houston, P.

MOX, Dipartimento di Matematica
Politecnico di Milano, Via Bonardi 9 - 20133 Milano (Italy)

mox-dmat@polimi.it http://mox.polimi.it

Review of Discontinuous Galerkin Finite Element Methods for Partial Differential Equations on Complicated Domains

Paola F. Antonietti[♯] Andrea Cangiani[♮] Joe Collis[♭]
Zhaonan Dong[♮] Emmanuil H. Georgoulis[†] Stefano Giani[§]
Paul Houston[♭]

June 8, 2015

[♯] MOX– Laboratory for Modeling and Scientific Computing, Dipartimento di Matematica, Politecnico di Milano Piazza Leonardo da Vinci 32, 20133 Milano, Italy.
paola.antonietti@polimi.it

[♮] Department of Mathematics, University of Leicester, Leicester LE1 7RH, UK.
Andrea.Cangiani@le.ac.uk,
zd14@le.ac.uk,

[♭] School of Mathematical Sciences, University of Nottingham, University Park, Nottingham, NG7 2RD, UK.
Joe.Collis@nottingham.ac.uk,
Paul.Houston@nottingham.ac.uk

[†]Department of Mathematics, University of Leicester, Leicester LE1 7RH, UK
and
School of Applied Mathematical and Physical Sciences, National Technical University of Athens, Athens 15780, Greece.
Emmanuil.Georgoulis@le.ac.uk

[§] School of Engineering and Computing Sciences, Durham University, South Road, Durham, DH1 3LE, UK.
Stefano.Giani@durham.ac.uk

Keywords: Discontinuous Galerkin finite element methods, polytopic elements, complicated domains.

Abstract

The numerical approximation of partial differential equations (PDEs) posed on complicated geometries, which include a large number of small geometrical features or microstructures, represents a challenging computational problem. Indeed, the use of standard mesh generators, employing

simplices or tensor product elements, for example, naturally leads to very fine finite element meshes, and hence the computational effort required to numerically approximate the underlying PDE problem may be prohibitively expensive. As an alternative approach, in this article we present a review of composite/agglomerated discontinuous Galerkin finite element methods (DGFEMs) which employ general polytopic elements. Here, the elements are typically constructed as the union of standard element shapes; in this way, the minimal dimension of the underlying composite finite element space is *independent* of the number of geometrical features. In particular, we provide an overview of *hp*–version inverse estimates and approximation results for general polytopic elements, which are sharp with respect to element facet degeneration. On the basis of these results, *a priori* error bounds for the *hp*–DGFEM approximation of both second–order elliptic and first–order hyperbolic PDEs will be derived. Finally, we present numerical experiments which highlight the practical application of DGFEMs on meshes consisting of general polytopic elements.

1 Introduction

In many application areas arising in engineering and biological sciences, for example, one is often required to numerically approximate partial differential equations (PDEs) posed on complicated domains which contain small (relative to the size of the overall domain) geometrical features, or so-called microstructures. The key underlying issue for all classes of finite element/finite volume methods is the design of a suitable computational mesh upon which the underlying PDE problem will be discretized. On the one hand, the mesh should provide an accurate description of the given geometry with a granularity sufficient to compute numerical approximations to within desired engineering accuracy constraints. On the other hand, the mesh should not be so fine that the computational time required to compute the desired solution is too high for practical turn-around times. These issues are particularly pertinent when high–order methods are employed, since in this setting it is desirable to employ relatively coarse meshes, so that the polynomial degree may be suitably enriched.

Standard mesh generators typically generate grids consisting of triangular/quadrilateral elements in two-dimensions and tetrahedral/hexahedral/prismatic/pyramidal elements in three-dimensions. On the basis of the mesh, in the traditional finite element setting, the underlying finite element space, consisting of (continuous/discontinuous) piecewise polynomials, is then constructed based on mapping polynomial bases defined on a canonical/reference element to the physical domain. In the presence of boundary layers, anisotropic meshing may be exploited; however, in areas of high curvature the use of such highly-stretched elements may lead to element self-intersection, unless the curvature of the geometry is carefully 'propagated' into the interior of the mesh through the use of isoparametric element mappings. The use of what we shall refer to as standard element shapes necessitates the exploitation of very fine computational meshes when the geom-

etry possesses small details or microstructures. Indeed, in such situations, an extremely large number of elements may be required for a given mesh generator to produce even a 'coarse' mesh which adequately describes the underlying geometry. Thereby, the solution of the resulting system of equations emanating, for example, from a finite element discretization of the underlying PDE on the resulting coarse mesh, may be impractical due to the large numbers of degrees of freedom involved. Moreover, since this initial coarse mesh already contains such a large number of elements, the use of efficient multilevel solvers may be difficult, as an adequate sequence of coarser grids which represent the geometry is unavailable. As an example arising in biological applications, in Figure 1, we show a finite element mesh of a porous scaffold employed for in vitro bone tissue growth, cf. [4, 5]. Here, the mesh, consisting of 3.2 million elements, has been generated based on μCT image data represented in the form of voxels.

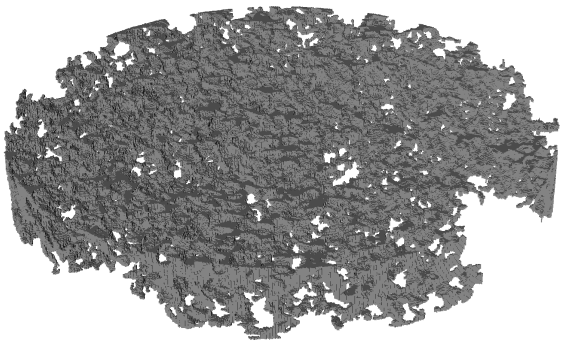

Figure 1: Example of a porous scaffold used for in vitro bone tissue growth, cf. [4, 5].

From the above discussion, we naturally conclude that, when standard element shapes are employed, the dimension of the underlying finite element space is proportional to the complexity of the given computational geometry. A natural alternative is to consider the exploitation of computational meshes consisting of general polytopic elements, i.e., polygons in two-dimensions and polyhedra in three-dimensions. In the context of discretizing PDEs in complicated geometries, Composite Finite Elements (CFEs) have been developed in the articles [33, 32] and [1, 31] for both conforming finite element and discontinuous Galerkin (DGFEM) methods, respectively, which exploit general meshes consisting of agglomerated elements consisting of a collection of neighbouring elements present within a standard finite element method. A closely related technique based on employing the so-called agglomerated DGFEM has also been considered in [7, 8, 9]. From a meshing point of view, the exploitation of general polytopic elements provides enormous flexibility. Indeed, in addition to meshing complicated geometries using a minimal number of elements, they are naturally suited to applications in complicated/moving domains, such as in solid mechanics, fluid

structure interaction, geophysical problems, including earthquake engineering and flows in fractured porous media, and mathematical biology, for example. Indeed, general element shapes are often exploited as transitional elements in finite element meshes, for example, when fictitious domain methods, unfitted methods or overlapping meshes are employed, cf. [16, 17, 18, 36, 39], for example. The use of similar techniques in the context of characteristic-based/Lagrange–Galerkin methods is also highly relevant. The practical relevance and potential impact of employing such general computational meshes is an extremely exciting topic which has witnessed a vast amount of intensive research in recent years by a number of leading research groups. In the conforming setting, we mention the CFE method [33, 32], the Polygonal Finite Element Method [45], and the Extended Finite Element Method [27]. These latter two approaches achieve conformity by enriching/modifying the standard polynomial finite element spaces, in the spirit of the Generalized Finite Element framework of Babuška & Osborn in [6]. Typically, the handling of non-standard shape functions carries an increase in computational effort. The recently proposed Virtual Element Method [11], overcomes this difficulty, achieving the extension of conforming finite element methods to polytopic elements while maintaining the ease of implementation of these schemes; see also the closely related Mimetic Finite Difference method, cf. [12, 14, 22], for example.

In this article we present an overview of CFEs, and in particular consider their construction and analysis within the *hp*–version DGFEM setting. With this in mind, we follow the work presented in [33, 32, 1]; the inclusion of general polytopic meshes which admit arbitrarily small/degenerate $(d-k)$–dimensional element facets, $k = 1, \ldots, d-1$, where d denotes the spatial dimension, will also be discussed, following [21, 20]. The structure of this article is as follows. In Section 2, we introduce composite/agglomerated DGFEMs for the numerical approximation of second–order elliptic PDEs. Section 3 is devoted to the stability and *a priori* analysis of the proposed method; in particular, we derive *hp*–version inverse estimates and approximation results which are sharp with respect to element facet degeneration. In Section 4 we analyze the *hp*–version DGFEM discretization of first–order hyperbolic PDEs on polytopic meshes. The practical performance of the proposed DGFEMs for application to incompressible fluid flow problems is studied in Section 5. Finally, in Section 6 we summarize the work presented in this article and draw some conclusions.

2 Construction of composite finite element methods

The original idea behind the construction of CFEs, as presented in [32, 33] for conforming finite element methods, is to exploit general shaped element domains upon which elemental basis functions may only be locally piecewise smooth. In particular, an element domain within a CFE may consist of a collection of neighbouring elements present within a standard finite element method, with

the basis function of the CFE being constructed as a linear combination of those defined on the standard finite element subdomains. The extension of this general approach to the DGFEM setting has been considered in the series of articles [1, 30, 31]; see also [2, 29] for their application within Schwarz-type domain decomposition preconditioners. For related work on the application of DGFEMs on meshes consisting of agglomerated elements, we refer to the articles [7, 8, 9]. We note that in the context of DGFEMs, the elemental finite element bases simply consist of polynomial functions, since inter-element conformity is not required.

For generality, we introduce CFE methods based on the construction proposed in [33] and [1]. Here, the philosophy underlying CFE methods is to construct finite element spaces based on first generating a hierarchy of meshes, such that the finest mesh does indeed provide an accurate representation of the underlying computational domain, followed by the introduction of appropriate prolongation operators which determine how the finite element basis functions on the coarse mesh are defined in terms of those on the fine grid. In this manner, CFEs naturally lend themselves to adaptive enrichment of the finite element space by locally varying the hierarchical level from which an element belongs, cf. [9, 31].

For concreteness, throughout this section, we concentrate on the numerical approximation of the Poisson equation. However, we stress that this class of methods naturally extends to a wide range of PDEs; indeed, it is the treatment of the underlying second–order PDE operator which gives rise to a number of theoretical and practical difficulties which we will address Section 3. With this in mind, given that Ω is a bounded, connected Lipschitz domain in $\mathbb{R}^d$, $d > 1$, with boundary $\partial\Omega$, consider the following PDE problem: find u such that

$$-\Delta u = f \quad \text{in } \Omega, \tag{1}$$

$$u = g \quad \text{on } \partial\Omega, \tag{2}$$

where $f \in L_2(\Omega)$ and g is a sufficiently regular boundary datum. In particular, it is assumed that Ω is a 'complicated' domain, in the sense that it contains small details or microstructures.

2.1 Composite/agglomerated meshes

The approach developed in [33], cf. also [1], is to construct the underlying physical/agglomerated meshes by first introducing a hierarchy of overlapping reference and logical meshes, from which a very fine geometry–conforming mesh, consisting of standard–shaped elements, may be defined, based on possibly moving nodes in the finest logical mesh onto the boundary $\partial\Omega$ of the computational domain. The coarse mesh, consisting of polytopic elements, is then constructed based on agglomerating elements which share the same parent within the underlying refinement tree.

More precisely, given an open bounded Lipschitz domain Ω, which potentially contains small features/microstructures, we first define the coarsest *reference* mesh $\mathcal{R}_H \equiv \mathcal{R}_{h_1}$ to be an overlapping grid in the sense that it does not resolve the boundary $\partial\Omega$ of the domain Ω. In particular, we let $\mathcal{R}_H = \{\hat{\kappa}\}$ be a coarse conforming shape–regular mesh consisting of (closed) standard element domains $\hat{\kappa}$, cf. above, whose open intersection is empty such that

$$\Omega \subset \Omega_H = \left(\bigcup_{\hat{\kappa} \in \mathcal{R}_H} \hat{\kappa} \right)^\circ \quad \text{and} \quad \hat{\kappa}^\circ \cap \Omega \neq \emptyset \ \ \forall \hat{\kappa} \in \mathcal{R}_H,$$

where, for a closed set $D \subset \mathbb{R}^d$, D° denotes the interior of D.

On the basis of the coarse mesh $\mathcal{R}_H$, a hierarchy of reference meshes $\mathcal{R}_{h_i}$, $i = 2, 3, \ldots, \ell$, are now constructed based on adaptively refining the coarse mesh $\mathcal{R}_H$ with a view to improving the approximation of the boundary of Ω. With this in mind, given an input tolerance TOL, we proceed as follows:

1. Set $\mathcal{R}_{h_1} = \mathcal{R}_H$, the mesh counter $i = 1$, and store the elements $\hat{\kappa} \in \mathcal{R}_{h_1}$ as the root nodes of the refinement tree $\hat{\mathfrak{T}}$; we assign these elements with a level number $L = 1$.

2. Writing children($\hat{\kappa}$) to denote the number of children that element $\hat{\kappa}$ possesses, construct the refinement set $\mathfrak{R}$:

$$\mathfrak{R} = \left\{ \hat{\kappa} \in \hat{\mathfrak{T}} : \ \text{children}(\hat{\kappa}) = 0 \ \ \wedge \ \ \hat{\kappa}^\circ \cap \partial\Omega \neq \emptyset \ \ \wedge \ \ h_{\hat{\kappa}} > \text{TOL} \right\}, \quad (3)$$

   where $h_{\hat{\kappa}} = \text{diam}(\hat{\kappa})$.

3. If $\mathfrak{R} = \emptyset$, then `STOP`. Otherwise, for each $\hat{\kappa} \in \mathfrak{R}$, refine the element $\hat{\kappa} = \bigcup_{i=1}^{n_{\hat{\kappa}}} \hat{\kappa}_i$. Here, we store the child elements $\hat{\kappa}_i$, $i = 1, \ldots, n_{\hat{\kappa}}$, within the tree $\hat{\mathfrak{T}}$, where $\hat{\kappa}$ is their parent, $\text{level}(\hat{\kappa}_i) = \text{level}(\hat{\kappa}) + 1$, $i = 1, \ldots, n_{\hat{\kappa}}$, and $\text{level}(\hat{\kappa})$ denotes the level of the element $\hat{\kappa}$ in $\hat{\mathfrak{T}}$. We point out that $n_{\hat{\kappa}}$ will depend on both the type of element to be refined, and the type of refinement, i.e., isotropic/anisotropic. For isotropic refinement of a quadrilateral element $\hat{\kappa}$ in two–dimensions, we have that $n_{\hat{\kappa}} = 4$.

4. Perform any additional refinements to undertake necessary mesh smoothing, for example, to ensure that the resulting mesh is 1–irregular, cf. [1].

5. Update mesh counter $i = i + 1$ and construct the reference mesh $\mathcal{R}_{h_i}$ from the tree structure $\hat{\mathfrak{T}}$ in the following manner:

$$\mathcal{R}_{h_i} \ = \ \left\{ \hat{\kappa} \in \hat{\mathfrak{T}} : \text{level}(\hat{\kappa}) = i \vee (\text{level}(\hat{\kappa}) \leq i \wedge \text{children}(\hat{\kappa}) = 0) \right\}.$$

6. Return to Step 2. and continue to iterate until either the condition in 3. is satisfied, or a maximum number of allowable refinements have been undertaken.

Remark 2.1. *We point out that the above procedure provides a generic refinement algorithm which may be employed to generate the sequence of reference meshes* $\{\mathcal{R}_{h_i}\}_{i=1}^{\ell}$*, though alternative sequences of hierarchical meshes may be exploited within the CFE framework.*

On the basis of the reference meshes $\{\mathcal{R}_{h_i}\}_{i=1}^{\ell}$, we now define the corresponding sequences of logical and physical meshes $\{\mathcal{L}_{h_i}\}_{i=1}^{\ell}$ and $\{\mathcal{M}_{h_i}\}_{i=1}^{\ell}$, respectively. To this end, we first consider the finest reference mesh $\mathcal{R}_{h_\ell}$: given that the stopping criterion in step 2. above, cf. (3), is satisfied, then vertex nodes $\hat{x}_v \in \hat{\kappa}$, $\hat{\kappa} \in \mathcal{R}_{h_\ell}$, which are close to the boundary $\partial\Omega$ in the sense that

$$\mathrm{dist}(\hat{x}_v, \partial\Omega) \ll h_{\hat{\kappa}},$$

are moved onto the boundary of the computational domain. As a result of this node movement procedure, some of the elements stored in the tree $\hat{\mathfrak{T}}$ may end up lying outside of Ω; these are subsequently removed from $\hat{\mathfrak{T}}$ to yield the cropped tree $\mathfrak{T}$. On the basis of the cropped tree data structure $\mathfrak{T}$, the logical meshes are constructed based on agglomerating elements which share a common parent within a given level of the mesh tree hierarchy $\mathfrak{T}$. More precisely, following [30], we introduce the following notation: for $\tilde{\kappa}_{\mathcal{C}} \in \mathfrak{T}$, with $\mathrm{level}(\tilde{\kappa}_{\mathcal{C}}) = j$, we write $\mathfrak{F}_i^j(\tilde{\kappa}_{\mathcal{C}})$, $j \geq i$, to denote the unique element $\tilde{\kappa}_{\mathcal{P}} \in \mathfrak{T}$ with $\mathrm{level}(\tilde{\kappa}_{\mathcal{P}}) = i$ who is directly related to $\tilde{\kappa}_{\mathcal{C}}$ in the sense that $\tilde{\kappa}_{\mathcal{C}} \subset \tilde{\kappa}_{\mathcal{P}}$; i.e., $\tilde{\kappa}_{\mathcal{C}}$ has resulted from subsequent refinement of $\tilde{\kappa}_{\mathcal{P}}$. In the trivial case when $j = i$, $\mathfrak{F}_i^j(\tilde{\kappa}_{\mathcal{C}}) = \tilde{\kappa}_{\mathcal{C}}$. Thereby, the logical meshes $\{\mathcal{L}_{h_i}\}_{i=1}^{\ell}$ may be constructed from $\mathfrak{T}$ as follows:

$$\begin{aligned}\mathcal{L}_{h_i} \quad = \quad & \{\tilde{\kappa} : (\tilde{\kappa} \in \mathfrak{T} \wedge \mathrm{level}(\tilde{\kappa}) \leq i \wedge \mathrm{children}(\tilde{\kappa}) = 0) \\ & \vee (\tilde{\kappa} = \cup_{\tilde{\kappa}' \in \mathfrak{T}} \tilde{\kappa}' : \mathrm{children}(\tilde{\kappa}') = 0 \ \wedge \mathfrak{F}_i^j(\tilde{\kappa}') = P, j = \mathrm{level}(\tilde{\kappa}') \\ & \quad \wedge P \text{ is identical for all members of this set})\}\,.\end{aligned}$$

We point out that in the absence of any node movement the finest reference and logical meshes $\mathcal{R}_{h_\ell}$ and $\mathcal{L}_{h_\ell}$, respectively, are identical.

Finally, the set of physical meshes $\{\mathcal{M}_{h_i}\}_{i=1}^{\ell}$ are defined based on moving the nodes in the respective logical meshes $\{\mathcal{L}_{h_i}\}_{i=1}^{\ell}$. More precisely, writing $\hat{\mathcal{N}}_\ell$ to denote the set of nodal points which define the finest logical mesh $\mathcal{L}_{h_\ell}$, the process of node movement naturally defines a bijective mapping

$$\Phi : \hat{\mathcal{N}}_\ell \to \mathcal{N}_\ell,$$

where $\mathcal{N}_\ell$ denotes the set of mapped vertex nodes. The mapping Φ can then be employed to map an element $\tilde{\kappa} \in \mathcal{L}_{h_\ell}$ to the physical element κ. For simplicity, we denote this mapping by Φ also; hence, we write

$$\Phi(\tilde{\kappa}) = \kappa.$$

With this notation, the physical meshes $\{\mathcal{M}_{h_i}\}_{i=1}^{\ell}$ may be defined as follows:

$$\mathcal{M}_{h_i} = \{\kappa : \kappa = \Phi(\tilde{\kappa}) \ \text{ for some } \ \tilde{\kappa} \in \mathcal{L}_{h_i}\},$$

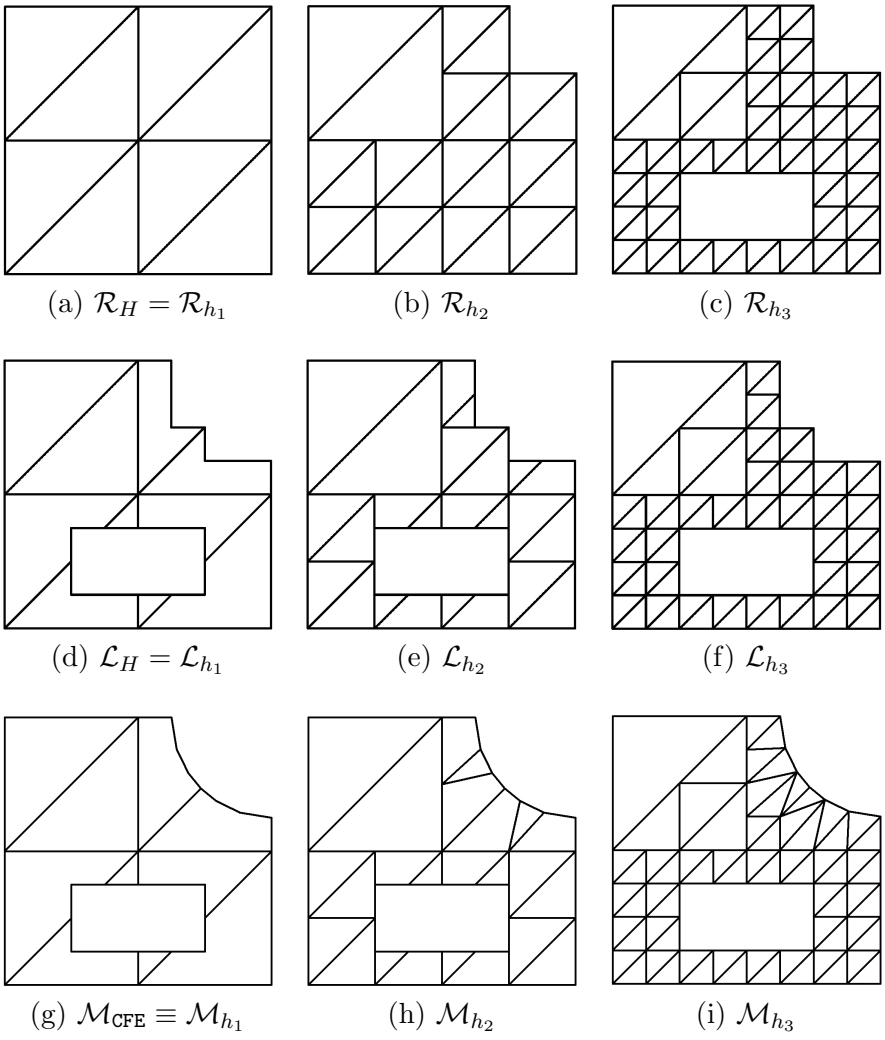

(a) $\mathcal{R}_H = \mathcal{R}_{h_1}$ (b) $\mathcal{R}_{h_2}$ (c) $\mathcal{R}_{h_3}$

(d) $\mathcal{L}_H = \mathcal{L}_{h_1}$ (e) $\mathcal{L}_{h_2}$ (f) $\mathcal{L}_{h_3}$

(g) $\mathcal{M}_{\mathtt{CFE}} \equiv \mathcal{M}_{h_1}$ (h) $\mathcal{M}_{h_2}$ (i) $\mathcal{M}_{h_3}$

Figure 2: Hierarchy of meshes: (a)–(c) Reference meshes; (d)–(f) Logical Meshes; (g)–(i) Corresponding physical meshes.

$i = 1, \ldots, \ell$. We point out that both the logical and physical meshes $\{\mathcal{L}_{h_i}\}_{i=1}^{\ell}$ and $\{\mathcal{M}_{h_i}\}_{i=1}^{\ell}$, respectively, may consist of general polygonal/polyhedral element domains. We refer to the coarsest physical mesh $\mathcal{M}_{h_1}$ as the CFE mesh, and accordingly write $\mathcal{M}_{\texttt{CFE}} \equiv \mathcal{M}_{h_1}$. As a simple example, in Figure 2, we consider the case when Ω is the unit square, which has had both the rectangular region $(1/4, 3/4) \times (1/8, 3/8)$ and the circular region enclosed by $r < 3/8$, where $r^2 = (x-1)^2 + (y-1)^2$, removed. Here, we show the reference, logical, and physical meshes $\{\mathcal{R}_{h_i}\}_{i=1}^{\ell}$, $\{\mathcal{L}_{h_i}\}_{i=1}^{\ell}$, and $\{\mathcal{M}_{h_i}\}_{i=1}^{\ell}$, respectively, when $\ell = 3$.

2.2 Finite element spaces

Given the set of physical (polytopic) meshes $\{\mathcal{M}_{h_i}\}_{i=1}^{\ell}$, constructed in the previous section, we introduce the corresponding sequence of DGFEM finite element spaces $V(\mathcal{M}_{h_i}, \mathbf{p}_i)$, $i = 1, \ldots, \ell$, respectively, consisting of piecewise discontinuous polynomials. To this end, for each element $\kappa \in \mathcal{M}_{\texttt{CFE}} (\equiv \mathcal{M}_{h_1})$, we associate a positive integer p_κ, henceforth referred to as the polynomial degree of the element $\kappa \in \mathcal{M}_{\texttt{CFE}}$, and collect the p_κ in the vector $\mathbf{p}_1 = (p_\kappa : \kappa \in \mathcal{M}_{\texttt{CFE}})$. The polynomial degree vectors $\mathbf{p}_i$, $i = 2, \ldots, \ell$, associated with the respective meshes $\mathcal{M}_{h_i}$, $i = 2, \ldots, \ell$, are then defined in such a manner that the polynomial degree of the child element contained within the refinement tree $\mathfrak{T}$ is directly inherited from its parent element. More precisely,

$$\mathbf{p}_i = (p_\kappa,\ \kappa \in \mathcal{M}_{h_i} : p_\kappa = p_{\kappa'},\ \text{where}\ \ \kappa' = \mathfrak{F}_1^j(\kappa)\ \ \wedge \text{level}(\kappa) = j,\ \kappa' \in \mathcal{M}_{\texttt{CFE}}).$$

With this in mind, we write

$$V(\mathcal{M}_{h_i}, \mathbf{p}_i) = \{u \in L_2(\Omega) : u|_\kappa \in \mathcal{P}_{p_\kappa}(\kappa)\ \forall \kappa \in \mathcal{M}_{h_i}\},$$

$i = 1, \ldots, \ell$, where $\mathcal{P}_p(\kappa)$ denotes the set of polynomials of degree at most $p \geq 1$ defined over the general polytope κ.

With this construction, noting that the meshes $\{\mathcal{M}_{h_i}\}_{i=1}^{\ell}$ are nested, we deduce that

$$V(\mathcal{M}_{h_1}, \mathbf{p}_1) \subset V(\mathcal{M}_{h_2}, \mathbf{p}_2) \subset \ldots \subset V(\mathcal{M}_{h_\ell}, \mathbf{p}_\ell).$$

We now introduce the classical prolongation (injection) operator from $V(\mathcal{M}_{h_i}, p)$ to $V(\mathcal{M}_{h_{i+1}}, p)$, $1 \leq i \leq \ell - 1$, given by

$$P_i^{i+1} : V(\mathcal{M}_{h_i}, \mathbf{p}_i) \to V(\mathcal{M}_{h_{i+1}}, \mathbf{p}_{i+1}), \quad i = 1, \ldots, \ell - 1.$$

Hence, the prolongation operator from $V(\mathcal{M}_{h_i}, \mathbf{p}_i)$ to $V(\mathcal{M}_{h_\ell}, \mathbf{p}_\ell)$, $1 \leq i \leq \ell - 1$, is defined by

$$P_i = P_{\ell-1}^{\ell} P_{\ell-2}^{\ell-1} \ldots P_i^{i+1}.$$

With this notation, we may write $V(\mathcal{M}_{h_i}, \mathbf{p}_i)$, $1 \leq i \leq \ell - 1$, in the following alternative manner

$$V(\mathcal{M}_{h_i}, \mathbf{p}_i) = \{u \in L_2(\Omega) : u = P_i^\top \phi,\ \phi \in V(\mathcal{M}_{h_\ell}, \mathbf{p}_\ell)\}, \tag{4}$$

where the restriction operator $P_i^\top$ is defined as the transpose of P_i, with respect to the standard $L_2(\Omega)$–inner product.

Remark 2.2. *The exploitation of the prolongation operator P_i within the definition of the finite element spaces $V(\mathcal{M}_{h_i}, \mathbf{p}_i)$, $i = 1, \ldots, \ell$, stated in (4) allows for the introduction of different spaces, depending on the specific choice of P_i. Here, cf. also [1], the finite element spaces are constructed so that on each (composite) element $\kappa \in \mathcal{M}_{h_i}$, $i = 1, \ldots, \ell$, the restriction of a function $v \in V(\mathcal{M}_{h_i}, \mathbf{p}_i)$ to κ is a polynomial of degree p_κ. In the case when the finite element spaces consist of continuous piecewise polynomials, cf. [33], for example, alternative prolongation operators are employed which leads to basis functions which are* piecewise *polynomials on each composite/polytopic element domain.*

The space $V(\mathcal{M}_{h_1}, \mathbf{p}_1) \equiv V(\mathcal{M}_{\mathtt{CFE}}, \boldsymbol{p})$ is referred to as the composite finite element space. We stress that the dimension of $V(\mathcal{M}_{\mathtt{CFE}}, \boldsymbol{p})$ is *independent* of the underlying domain Ω in the sense that it does not directly depend on the number of microstructures contained in Ω. Indeed, the dimension of $V(\mathcal{M}_{\mathtt{CFE}}, \boldsymbol{p})$ can be chosen by the user; of course, if $V(\mathcal{M}_{\mathtt{CFE}}, \boldsymbol{p})$ is not sufficiently rich, then the accuracy of any computed finite element approximation $u_h \in V(\mathcal{M}_{\mathtt{CFE}}, \boldsymbol{p})$ may be low. However, given the construction of the composite finite element mesh $\mathcal{M}_{\mathtt{CFE}}$, the underlying numerical scheme naturally lends itself to adaptive enrichment of the finite element space $V(\mathcal{M}_{\mathtt{CFE}}, \boldsymbol{p})$, cf. [31, 30].

Remark 2.3. *As a final remark, we note that an alternative approach for the construction of the composite finite element mesh $\mathcal{M}_{\mathtt{CFE}}$ is to simply employ a standard mesh generator to produce a fine mesh $\mathcal{M}_{fine}$ which accurately describes the domain Ω. Then coarse agglomerated meshes may be constructed based on employing graph partitioning algorithms. One of the most popular software packages employed for this purpose is METIS [37], cf. [20, 29]. From a theoretical point of view, this setting is more difficult to analyse; we shall return to this issue in Section 3.*

To define the forthcoming DGFEM, cf. Section 2.3, we define the broken Sobolev space $H^{\mathbf{k}}(\Omega, \mathcal{M}_{\mathtt{CFE}})$ with respect to the subdivision $\mathcal{M}_{\mathtt{CFE}}$ up to composite order $\mathbf{k}$ in the standard fashion:

$$H^{\mathbf{k}}(\Omega, \mathcal{M}_{\mathtt{CFE}}) = \{u \in L_2(\Omega) : u|_\kappa \in H^{k_\kappa}(\kappa) \quad \forall \kappa \in \mathcal{M}_{\mathtt{CFE}}\}.$$

Moreover, for $u \in H^1(\Omega, \mathcal{M}_{\mathtt{CFE}})$, we define the broken gradient $\nabla_h u$ by $(\nabla_h u)|_\kappa = \nabla(u|_\kappa), \kappa \in \mathcal{M}_{\mathtt{CFE}}$.

2.3 Discontinuous Galerkin methods on polytopic meshes

In this section, we consider the DGFEM discretization of the second-order elliptic PDE model problem (1)–(2). For concreteness, we focus our attention on the *hp*-version of the (symmetric) interior penalty DGFEM.

For the proceeding analysis, we introduce the concept of mesh interfaces and faces, cf. [21]. In order to admit hanging nodes/edges, which are permitted in $\mathcal{M}_{\texttt{CFE}}$, the interfaces of $\mathcal{M}_{\texttt{CFE}}$ are defined to be the intersection of the $(d-1)$–dimensional facets of neighbouring elements; on the boundary an interface is simply a $(d-1)$–dimensional facet of $\kappa \in \mathcal{M}_{\texttt{CFE}}$. In the two–dimensional setting, i.e., $d = 2$, the interfaces of a given element $\kappa \in \mathcal{M}_{\texttt{CFE}}$ simply consists of line segments ($(d-1)$–dimensional simplices). For $d = 3$, we assume that each interface of an element $\kappa \in \mathcal{M}_{\texttt{CFE}}$ may be subdivided into a set of co-planar triangles; we use the terminology 'face' to refer to a $(d-1)$–dimensional simplex (line segment or triangle for $d = 2$ or 3, respectively), which forms part of the boundary (interface) of an element $\kappa \in \mathcal{M}_{\texttt{CFE}}$. For $d = 2$, the face and interface of an element $\kappa \in \mathcal{M}_{\texttt{CFE}}$ coincide.

Following [20, 21], we assume that a sub-triangulation into faces of each mesh interface is given if $d = 3$, and denote by $\mathcal{F}_{\texttt{CFE}}$ the union of all open mesh interfaces if $d = 2$ and the union of all open triangles belonging to the sub-triangulation of all mesh interfaces if $d = 3$. In this way, $\mathcal{F}_{\texttt{CFE}}$ is always defined as a set of $(d-1)$–dimensional simplices. Further, we write $\mathcal{F}_{\texttt{CFE}} = \mathcal{F}^{\mathcal{I}}_{\texttt{CFE}} \cup \mathcal{F}^{\mathcal{B}}_{\texttt{CFE}}$, where $\mathcal{F}^{\mathcal{I}}_{\texttt{CFE}}$ denotes the union of all open $(d-1)$–dimensional element faces $F \subset \mathcal{F}_{\texttt{CFE}}$ that are contained in Ω, and $\mathcal{F}^{\mathcal{B}}_{\texttt{CFE}}$ is the union of element boundary faces, i.e., $F \subset \partial\Omega$ for $F \in \mathcal{F}^{\mathcal{B}}_{\texttt{CFE}}$. The boundary $\partial\kappa$ of an element κ and the sets $\partial\kappa \setminus \partial\Omega$ and $\partial\kappa \cap \partial\Omega$ will be identified in a natural way with the corresponding subsets of $\mathcal{F}_{\texttt{CFE}}$.

Given $\kappa \in \mathcal{M}_{\texttt{CFE}}$, the trace of a function $v \in H^1(\Omega, \mathcal{M}_{\texttt{CFE}})$ on $\partial\kappa$, relative to κ, is denoted by v^+_κ. Then for almost every $\mathbf{x} \in \partial\kappa \backslash \partial\Omega$, there exists a unique $\kappa' \in \mathcal{M}_{\texttt{CFE}}$ such that $\mathbf{x} \in \partial\kappa'$; with this notation, the outer/exterior trace v^-_κ of v on $\partial\kappa \backslash \partial\Omega$, relative to κ, is defined as the inner trace $v^+_{\kappa'}$ relative to the element(s) κ' such that the intersection of $\partial\kappa'$ with $\partial\kappa \backslash \partial\Omega$ has positive $(d-1)$–dimensional measure.

Next, we introduce some additional trace operators. Let κ_i and κ_j be two adjacent elements of $\mathcal{M}_{\texttt{CFE}}$ and let $\mathbf{x}$ be an arbitrary point on the interior face $F \in \mathcal{F}^{\mathcal{I}}_{\texttt{CFE}}$ given by $F = \partial\kappa_i \cap \partial\kappa_j$. We write $\mathbf{n}_i$ and $\mathbf{n}_j$ to denote the outward unit normal vectors on F, relative to $\partial\kappa_i$ and $\partial\kappa_j$, respectively. Furthermore, let v and $\mathbf{q}$ be scalar- and vector-valued functions, which are smooth inside each element κ_i and κ_j. By $(v_i, \mathbf{q}_i)$ and $(v_j, \mathbf{q}_j)$, we denote the traces of $(v, \mathbf{q})$ on F taken from within the interior of κ_i and κ_j, respectively. The averages of v and $\mathbf{q}$ at $\mathbf{x} \in F \in \mathcal{F}^{\mathcal{I}}_{\texttt{CFE}}$ are given by

$$\{\!\{v\}\!\} = \frac{1}{2}(v_i + v_j), \quad \{\!\{\mathbf{q}\}\!\} = \frac{1}{2}(\mathbf{q}_i + \mathbf{q}_j),$$

respectively. Similarly, the jumps of v and $\mathbf{q}$ at $\mathbf{x} \in F \in \mathcal{F}^{\mathcal{I}}_{\texttt{CFE}}$ are given by

$$[\![v]\!] = v_i\,\mathbf{n}_i + v_j\,\mathbf{n}_j, \quad [\![\mathbf{q}]\!] = \mathbf{q}_i \cdot \mathbf{n}_i + \mathbf{q}_j \cdot \mathbf{n}_j,$$

respectively. On a boundary face $F \in \mathcal{F}^{\mathcal{B}}_{\texttt{CFE}}$, such that $F \subset \partial\kappa_i$, $\kappa_i \in \mathcal{M}_{\texttt{CFE}}$, we

set

$$\{\!\{v\}\!\} = v_i, \quad \{\!\{\mathbf{q}\}\!\} = \mathbf{q}_i, \quad [\![v]\!] = v_i \mathbf{n}_i \quad [\![\mathbf{q}]\!] = \mathbf{q}_i \cdot \mathbf{n}_i,$$

with $\mathbf{n}_i$ denoting the unit outward normal vector on the boundary $\partial\Omega$.

With this notation, the symmetric interior penalty DGFEM for the numerical approximation of (1)–(2) is given by: find $u_h \in V(\mathcal{M}_{\mathtt{CFE}}, \boldsymbol{p})$ such that

$$B_{\mathtt{Diff}}(u_h, v_h) = F_{\mathtt{Diff}}(v_h) \tag{5}$$

for all $v_h \in V(\mathcal{M}_{\mathtt{CFE}}, \boldsymbol{p})$, where

$$\begin{aligned} B_{\mathtt{Diff}}(w, v) = & \sum_{\kappa \in \mathcal{M}_{\mathtt{CFE}}} \int_\kappa \nabla w \cdot \nabla v \, d\mathbf{x} - \sum_{F \in \mathcal{F}_{\mathtt{CFE}}} \int_F \left(\{\!\{\nabla_h v\}\!\} \cdot [\![w]\!] + \{\!\{\nabla_h w\}\!\} \cdot [\![v]\!] \right) ds \\ & + \sum_{F \in \mathcal{F}_{\mathtt{CFE}}} \int_F \sigma \, [\![w]\!] \cdot [\![v]\!] \, ds, \\ F_{\mathtt{Diff}}(v) = & \int_\Omega f v \, d\mathbf{x} - \sum_{F \in \mathcal{F}^{\mathcal{B}}_{\mathtt{CFE}}} \int_F g(\nabla_h v \cdot \mathbf{n} - \sigma v) \, \mathrm{d}s. \end{aligned}$$

Here, the non-negative function $\sigma \in L_\infty(\mathcal{F}_{\mathtt{CFE}})$ is the discontinuity stabilization function; the precise definition of σ is given in Lemma 3.4 below.

3 Stability and approximation results

In this section we consider the stability and error analysis of the *hp*–version DGFEM defined in (5). We point out that the original *a priori* error analysis of the DGFEM (5) on CFE meshes was first undertaken in the article [1], based on exploiting the work developed in both the CFE and DGFEM settings in the articles [33] and [35], respectively. Indeed, the analysis presented in [1] was based on bounding the error in terms of Sobolev norms of an extension, cf. Theorem 3.1 below, of the analytical solution u from an element belonging to the logical mesh to its respective element in the reference mesh, assuming the mapping Φ is sufficiently regular. This approach is advantageous since the (coarsest) reference mesh $\mathcal{R}_{h_1}$ consists of non-overlapping standard–shaped elements. In order to treat general polytopes, where an underlying reference and logical mesh may not be available, for example, on meshes generated from graph partitioning software, cf. Remark 2.3, we proceed based on employing the recent analysis developed in [21].

In contrast to the case when standard element domains are employed, the exploitation of general polytopic elements presents a number of key challenges for the construction and analysis of stable numerical schemes. In particular, shape–regular polytopes may admit arbitrarily small/degenerate $(d-k)$–dimensional element facets, $k = 1, \ldots, d-1$, under mesh refinement, where d denotes the spatial dimension. Thereby, standard inverse and approximation results must be carefully extended to the polytopic setting in such a manner that the resulting

bounds are indeed sharp with respect to facet degeneration. With this in mind, we now summarise a number of key results derived in [21].

Firstly, we outline the key assumptions on the underlying CFE mesh $\mathcal{M}_{\mathtt{CFE}}$.

Assumption 3.1. *There exists a positive constant C_F, independent of the mesh parameters, such that*

$$\max_{\kappa\in\mathcal{M}_{\mathtt{CFE}}} \left(card\{F \in \mathcal{F}_{\mathtt{CFE}} : F \subset \partial\kappa\}\right) \leq C_F.$$

In order to deal with the case of general polytopic meshes, i.e., when reference/logical meshes are not available, we need to assume the existence of the following coverings of the mesh.

Definition 3.1. *A* covering $\mathcal{T}_\sharp = \{\mathcal{K}\}$ *related to the polytopic mesh $\mathcal{M}_{\mathtt{CFE}}$ is a set of shape-regular d–simplices $\mathcal{K}$, such that for each $\kappa \in \mathcal{M}_{\mathtt{CFE}}$, there exists a $\mathcal{K} \in \mathcal{T}_\sharp$ such that $\kappa \subset \mathcal{K}$. Given $\mathcal{T}_\sharp$, we denote by $\Omega_\sharp$ the* covering domain *given by $\Omega_\sharp = \left(\cup_{\mathcal{K}\in\mathcal{T}_\sharp}\bar{\mathcal{K}}\right)^\circ$.*

Assumption 3.2. *There exists a covering $\mathcal{T}_\sharp$ of $\mathcal{M}_{\mathtt{CFE}}$ and a positive constant $\mathcal{O}_\Omega$, independent of the mesh parameters, such that*

$$\max_{\kappa\in\mathcal{M}_{\mathtt{CFE}}} \mathcal{O}_\kappa \leq \mathcal{O}_\Omega,$$

where, for each $\kappa \in \mathcal{M}_{\mathtt{CFE}}$,

$$\mathcal{O}_\kappa = card\left\{\kappa' \in \mathcal{M}_{\mathtt{CFE}} : \kappa' \cap \mathcal{K} \neq \emptyset,\ \mathcal{K} \in \mathcal{T}_\sharp \ \ such\ that\ \ \kappa \subset \mathcal{K}\right\}.$$

Thereby,

$$\mathrm{diam}(\mathcal{K}) \leq C_{\mathrm{diam}} h_\kappa,$$

for each pair $\kappa \in \mathcal{M}_{\mathtt{CFE}}$, $\mathcal{K} \in \mathcal{T}_\sharp$, with $\kappa \subset \mathcal{K}$, for a constant $C_{\mathrm{diam}} > 0$, uniformly with respect to the mesh size.

Remark 3.1. *We note that for the classes of meshes constructed in Section 2.1, the coarsest reference mesh, subject to the (potential) application of the mapping Φ, may serve as the covering mesh $\mathcal{T}_\sharp$; in this setting Assumption 3.2 is trivially satisfied.*

The proceeding *hp*–approximation results and inverse estimates for polytopic elements are based on considering d–dimensional simplices, where standard results can be applied. With this in mind, we introduce the following element submesh.

Definition 3.2. *For each element κ in the computational mesh $\mathcal{M}_{\mathtt{CFE}}$, we define the family $\mathcal{F}_\flat^\kappa$ of all possible d–dimensional simplices contained in κ and having at least one face in common with κ. The notation $\kappa_\flat^F$ will be used to indicate a simplex belonging to $\mathcal{F}_\flat^\kappa$ and sharing with $\kappa \in \mathcal{M}_{\mathtt{CFE}}$ a given face F.*

Equipped with these results, we first consider the derivation of *hp*–version inverse estimates on general polytopes.

3.1 Inverse estimates

Inverse estimates, which bound a norm of a polynomial on an element face by a norm on the element itself, are fundamental for the study of the stability and error analysis of DGFEMs. In order to derive bounds which are sharp with respect to small/degenerate $(d-k)$–dimensional element facets, $k = 1, \ldots, d-1$, we first introduce the following definition.

Definition 3.3. *Let $\widetilde{\mathcal{M}}_{\mathtt{CFE}}$ denote the subset of elements κ, $\kappa \in \mathcal{M}_{\mathtt{CFE}}$, such that each $\kappa \in \widetilde{\mathcal{M}}_{\mathtt{CFE}}$ can be covered by at most $m_{\mathcal{M}_{\mathtt{CFE}}}$ shape-regular simplices K_i, $i = 1, \ldots, m_{\mathcal{M}_{\mathtt{CFE}}}$, such that*

$$\operatorname{dist}(\kappa, \partial K_i) < C_{as} \operatorname{diam}(K_i)/p_\kappa^2,$$

and

$$|K_i| \geq c_{as}|\kappa|$$

for all $i = 1, \ldots, m_{\mathcal{M}_{\mathtt{CFE}}}$, for some $m_{\mathcal{M}_{\mathtt{CFE}}} \in \mathbb{N}$ and $C_{as}, c_{as} > 0$, independent of κ and $\mathcal{M}_{\mathtt{CFE}}$.

We now state the main result of this section; see [21] for details of the proof.

Lemma 3.1. *Let $\kappa \in \mathcal{M}_{\mathtt{CFE}}$, $F \subset \partial\kappa$ denote one of its faces, and $\widetilde{\mathcal{M}}_{\mathtt{CFE}}$ be defined as in Definition 3.3. Then, for each $v \in \mathcal{P}_p(\kappa)$, we have the inverse estimate*

$$\|v\|_{L_2(F)}^2 \leq C_{\mathrm{INV}}(p, \kappa, F) \frac{p^2|F|}{|\kappa|} \|v\|_{L_2(\kappa)}^2, \tag{6}$$

with

$$C_{\mathrm{INV}}(p, \kappa, F) := C_{\mathrm{inv}} \begin{cases} \min\left\{ \dfrac{|\kappa|}{\sup_{\kappa_\flat^F \subset \kappa} |\kappa_\flat^F|}, p^{2d} \right\}, & \text{if } \kappa \in \widetilde{\mathcal{M}}_{\mathtt{CFE}}, \\ \dfrac{|\kappa|}{\sup_{\kappa_\flat^F \subset \kappa} |\kappa_\flat^F|}, & \text{if } \kappa \in \mathcal{M}_{\mathtt{CFE}} \backslash \widetilde{\mathcal{M}}_{\mathtt{CFE}}, \end{cases}$$

and $\kappa_\flat^F \in \mathcal{F}_\flat^\kappa$ as in Definition 3.2. Furthermore, C_{inv} is a positive constant, which if $\kappa \in \widetilde{\mathcal{M}}_{\mathtt{CFE}}$ depends on the shape regularity of the covering of κ given in Definition 3.3, but is always independent of $|\kappa|/\sup_{\kappa_\flat^F \subset \kappa} |\kappa_\flat^F|$ (and, therefore, of $|F|$), p, and v.

Remark 3.2. *Loosely speaking, the proof of Lemma 3.1 is based on exploiting standard inverse inequalities, cf. [43], for example, together with Definition 3.3. Indeed, for $\kappa \in \widetilde{\mathcal{M}}_{\mathtt{CFE}}$, the essential idea is to derive two bounds, one based on extending results from [28], and one based on employing an $L_\infty(\kappa)$ bound. Taking the minimum of these two bounds gives rise to an inverse inequality which is both sharp with respect to the polynomial degree p, and moreover is sensitive with respect to the measure of the face F relative to that of the element κ.*

We finish this section by recalling the inverse estimate for the H^1-(semi)norm derived in [20], cf. also [3]. In this setting, the shape regularity assumption on the covering $\mathcal{T}_\sharp$, cf. Definition 3.1, must be strengthened as follows.

Assumption 3.3. *The subdivision $\mathcal{M}_{\mathtt{CFE}}$ is shape regular in the sense of [24], i.e., there exists a positive constant C_{shape}, independent of the mesh parameters, such that:*

$$\forall \kappa \in \mathcal{M}_{\mathtt{CFE}}, \quad \frac{h_\kappa}{\rho_\kappa} \leq C_{\text{shape}},$$

with ρ_κ denoting the diameter of the largest ball contained in κ.

Following, [20], we also require the following assumption.

Assumption 3.4. *Every polytopic element $\kappa \in \mathcal{M}_{\mathtt{CFE}} \backslash \widetilde{\mathcal{M}}_{\mathtt{CFE}}$, admits a sub-triangulation into at most $n_{\mathcal{M}_{\mathtt{CFE}}}$ shape-regular simplices k_i, $i = 1, 2, \ldots, n_{\mathcal{M}_{\mathtt{CFE}}}$, such that $\bar{\kappa} = \cup_{i=1}^{n_{\mathcal{M}_{\mathtt{CFE}}}} \bar{k}_i$ and*

$$|k_i| \geq \hat{c}|\kappa|$$

for all $i = 1, \ldots, n_{\mathcal{M}_{\mathtt{CFE}}}$, for some $n_{\mathcal{M}_{\mathtt{CFE}}} \in \mathbb{N}$ and $\hat{c} > 0$, independent of κ and $\mathcal{M}_{\mathtt{CFE}}$.

Lemma 3.2. *Given Assumptions 3.3 and 3.4 are satisfied, for each $v \in \mathcal{P}_p(\kappa)$, the following inverse inequality holds*

$$\|\nabla v\|^2_{L_2(\kappa)} \leq \tilde{C}_{\text{inv}} \frac{p^4}{h^2_\kappa} \|v\|^2_{L_2(\kappa)}, \tag{7}$$

where $\tilde{C}_{\text{inv}}$ is a positive constant, independent of the element diameter h_κ and the polynomial order p_κ, but dependent on the shape regularity of the covering of κ, if $\kappa \in \widetilde{\mathcal{M}}_{\mathtt{CFE}}$, or the sub-triangulation of κ, if $\kappa \in \mathcal{M}_{\mathtt{CFE}} \backslash \widetilde{\mathcal{M}}_{\mathtt{CFE}}$.

3.2 Approximation results

Functions defined on Ω can be extended to the covering domain $\Omega_\sharp$ based on employing the following extension operator, cf. [44].

Theorem 3.1. *Let Ω be a domain with a Lipschitz boundary. Then there exists a linear extension operator $\mathcal{E} : H^s(\Omega) \to H^s(\mathbb{R}^d)$, $s \in \mathbb{N}_0$, such that $\mathcal{E}v|_\Omega = v$ and*

$$\|\mathcal{E}v\|_{H^s(\mathbb{R}^d)} \leq C\|v\|_{H^s(\Omega)},$$

where C is a positive constant depending only on s and Ω.

We point out that the assumptions stated in Theorem 3.1 on the domain Ω may be weakened. Indeed, [44] only requires that Ω is a domain with a minimally smooth boundary; the extension to domains which are simply connected, but may contain microscales, is treated in [42].

With the above notation, we now quote Lemma 4.2 from [21].

Lemma 3.3. *Let $\kappa \in \mathcal{M}_{\mathtt{CFE}}$, $F \subset \partial\kappa$ denote one of its faces, and $\mathcal{K} \in \mathcal{T}_\sharp$ denote the corresponding simplex such that $\kappa \subset \mathcal{K}$, cf. Definition 3.1. Suppose that $v \in L_2(\Omega)$ is such that $\mathcal{E}v|_{\mathcal{K}} \in H^{k_\kappa}(\mathcal{K})$, for some $k \geq 0$. Then, given Assumption 3.2 is satisfied, there exists $\tilde{\Pi}v$, such that $\tilde{\Pi}v|_\kappa \in \mathcal{P}_{p_\kappa}(\kappa)$, and the following bounds hold*

$$\|v - \tilde{\Pi}v\|_{H^q(\kappa)} \leq C \frac{h_\kappa^{s_\kappa - q}}{p_\kappa^{k_\kappa - q}} \|\mathcal{E}v\|_{H^{k_\kappa}(\mathcal{K})}, \quad k_\kappa \geq 0,$$

for $0 \leq q \leq k_\kappa$, and

$$\|v - \tilde{\Pi}v\|_{L_2(F)} \leq C|F|^{1/2} \frac{h_\kappa^{s_\kappa - d/2}}{p_\kappa^{k_\kappa - 1/2}} C_m(p_\kappa, \kappa, F)^{1/2} \|\mathcal{E}v\|_{H^{k_\kappa}(\mathcal{K})}, \quad k_\kappa > d/2,$$

where

$$C_m(p_\kappa, \kappa, F) = \min\left\{ \frac{h_\kappa^d}{\sup_{\kappa_\flat^F \subset \kappa} |\kappa_\flat^F|}, \frac{1}{p_\kappa^{1-d}} \right\}.$$

Here, $s_\kappa = \min\{p_\kappa + 1, k_\kappa\}$ and C is a positive constant, which depends on the shape-regularity of $\mathcal{K}$, but is independent of v, h_κ, and p_κ.

3.3 Error analysis of the DGFEM

On the basis of the results stated in Sections 3.1 & 3.2, we now proceed with the stability and error analysis of the DGFEM defined in (5). To this end, following the work presented in [40], we begin by defining the following extensions of the forms $B_{\mathtt{Diff}}(\cdot,\cdot)$ and $F_{\mathtt{Diff}}(\cdot)$:

$$\begin{aligned}
\tilde{B}_{\mathtt{Diff}}(w,v) = &\sum_{\kappa \in \mathcal{M}_{\mathtt{CFE}}} \int_\kappa \nabla w \cdot \nabla v \, d\mathbf{x} + \sum_{F \in \mathcal{F}_{\mathtt{CFE}}} \int_F \sigma \, [\![w]\!] \cdot [\![v]\!] \, ds \\
&- \sum_{F \in \mathcal{F}_{\mathtt{CFE}}} \int_F \left(\{\!\{ \boldsymbol{\Pi}_2(\nabla_h v) \}\!\} \cdot [\![w]\!] + \{\!\{ \boldsymbol{\Pi}_2(\nabla_h w) \}\!\} \cdot [\![v]\!] \right) ds, \\
\tilde{F}_{\mathtt{Diff}}(v) = &\int_\Omega f v \, d\mathbf{x} - \sum_{F \in \mathcal{F}_{\mathtt{CFE}}^{\mathcal{B}}} \int_F g (\boldsymbol{\Pi}_2(\nabla_h v) \cdot \mathbf{n} - \sigma v) \, \mathrm{d}s,
\end{aligned}$$

respectively. Here, $\boldsymbol{\Pi}_2 : [L_2(\Omega)]^d \to [V(\mathcal{M}_{\mathtt{CFE}}, \boldsymbol{p})]^d$ denotes the orthogonal L_2-projection onto the finite element space $[V(\mathcal{M}_{\mathtt{CFE}}, \boldsymbol{p})]^d$. Thereby, face integrals involving the terms $\{\!\{ \boldsymbol{\Pi}_2(\nabla_h w) \}\!\}$, $\{\!\{ \boldsymbol{\Pi}_2(\nabla_h v) \}\!\}$ and $\boldsymbol{\Pi}_2(\nabla_h v)$ are well defined for all $v, w \in \mathcal{S} = H^1(\Omega) + V(\mathcal{M}_{\mathtt{CFE}}, \boldsymbol{p})$, as these terms are now traces of elementwise polynomial functions. Moreover, it is clear that

$$\tilde{B}_{\mathtt{Diff}}(w,v) = B_{\mathtt{Diff}}(w,v) \qquad \text{for all} \quad w, v \in V(\mathcal{M}_{\mathtt{CFE}}, \boldsymbol{p}),$$

and

$$\tilde{F}_{\mathtt{Diff}}(v) = F_{\mathtt{Diff}}(v) \qquad \text{for all} \quad v \in V(\mathcal{M}_{\mathtt{CFE}}, \boldsymbol{p}).$$

Hence, we may rewrite the discrete problem (5) in the following equivalent manner: find $u_h \in V(\mathcal{M}_{\mathtt{CFE}}, \boldsymbol{p})$ such that

$$\tilde{B}_{\mathtt{Diff}}(u_h, v_h) = \tilde{F}_{\mathtt{Diff}}(v_h) \qquad \forall v_h \in V(\mathcal{M}_{\mathtt{CFE}}, \boldsymbol{p}). \tag{8}$$

Given the discrete nature of the L_2–projection operator $\boldsymbol{\Pi}_2$, the DGFEM formulation (8) is no longer consistent.

For the proceeding error analysis, we introduce the DG-norm $|||\cdot|||_{\mathtt{Diff}}$ by

$$|||w|||_{\mathtt{Diff}} = \Big(\sum_{\kappa \in \mathcal{M}_{\mathtt{CFE}}} \int_\kappa |\nabla w|^2 \,\mathrm{d}\mathbf{x} + \sum_{F \in \mathcal{F}_{\mathtt{CFE}}} \int_F \sigma |[\![w]\!]|^2 \,\mathrm{d}s \Big)^{1/2},$$

for $w \in \mathcal{S}$ and $\sigma > 0$.

With this notation, we recall the following coercivity and continuity properties of the bilinear form $\tilde{B}_{\mathtt{Diff}}(\cdot,\cdot)$ derived in [21].

Lemma 3.4. *Let $\sigma : \mathcal{F}_{\mathtt{CFE}} \to \mathbb{R}_+$ be defined facewise by*

$$\sigma(\mathbf{x}) = \begin{cases} C_\sigma \max\limits_{\kappa \in \{\kappa^+, \kappa^-\}} \Big\{ C_{\mathrm{INV}}(p_\kappa, \kappa, F) \dfrac{p_\kappa^2 |F|}{|\kappa|} \Big\}, & \mathbf{x} \in F \in \mathcal{F}_{\mathtt{CFE}}^{\mathcal{I}},\ F = \partial\kappa^+ \cap \partial\kappa^-, \\ C_\sigma C_{\mathrm{INV}}(p_\kappa, \kappa, F) \dfrac{p_\kappa^2 |F|}{|\kappa|}, & \mathbf{x} \in F \in \mathcal{F}_{\mathtt{CFE}}^{\mathcal{B}},\ F = \partial\kappa \cap \partial\Omega, \end{cases} \tag{9}$$

with $C_\sigma > 0$ large enough, depending on C_F, and independent of p, $|F|$, and $|\kappa|$. Then, given Assumption 3.1 holds, we have that

$$\tilde{B}_{\mathtt{Diff}}(v, v) \geq C_{\mathrm{coer}} |||v|||_{\mathtt{Diff}}^2 \quad \textit{for all} \quad v \in \mathcal{S},$$

and

$$\tilde{B}_{\mathtt{Diff}}(w, v) \leq C_{\mathrm{cont}} |||w|||_{\mathtt{Diff}} \, |||v|||_{\mathtt{Diff}} \quad \textit{for all} \quad w, v \in \mathcal{S},$$

where C_{coer} and C_{cont} are positive constants, independent of the discretization parameters.

Remark 3.3. *We point out that Lemma 3.4 assumes that the number of element faces remains bounded under mesh refinement, cf. Assumption 3.1. However, based on the computations undertaken in [3], in practice we observe that C_{coer} remains uniformly bounded on sequences of agglomerated polygons which violate this condition. Indeed, for $C_\sigma = 10$ numerical experiments suggest that $C_{\mathrm{coer}} \geq 0.8$.*

Given the definition of the discontinuity stabilization function σ stated in Lemma 3.4, we now state the following *a priori* error bound.

Theorem 3.2. *Let $\Omega \subset \mathbb{R}^d$, $d = 2, 3$, be a bounded polyhedral domain, and let $\mathcal{M}_{\mathtt{CFE}} = \{\kappa\}$ be a subdivision of Ω consisting of general polytopic elements*

satisfying Assumption 3.1. Further, $\mathcal{T}_\sharp = \{\mathcal{K}\}$ denotes the associated covering of Ω consisting of shape-regular d–simplices as in Definition 3.1, satisfying Assumption 3.2. Let $u_h \in V(\mathcal{M}_{\mathtt{CFE}}, \boldsymbol{p})$ be the DGFEM approximation to $u \in H^1(\Omega)$ defined by (5) with the discontinuity stabilization parameter given by (9), and suppose that $u|_\kappa \in H^{k_\kappa}(\kappa)$, $k_\kappa > 1 + d/2$, for each $\kappa \in \mathcal{M}_{\mathtt{CFE}}$, such that $\mathcal{E}u|_{\mathcal{K}} \in H^{k_\kappa}(\mathcal{K})$, where $\mathcal{K} \in \mathcal{T}_\sharp$ with $\kappa \subset \mathcal{K}$. Then, the following bound holds:

$$|||u - u_h|||^2_{\mathtt{Diff}} \leq C \sum_{\kappa \in \mathcal{M}_{\mathtt{CFE}}} \frac{h_\kappa^{2(s_\kappa - 1)}}{p_\kappa^{2(k_\kappa - 1)}} \left(1 + \mathcal{G}_\kappa(F, C_{\mathrm{INV}}, C_m, p_\kappa)\right) \|\mathcal{E}u\|^2_{H^{k_\kappa}(\mathcal{K})},$$

where

$$\begin{aligned}\mathcal{G}_\kappa(F, C_{\mathrm{INV}}, C_m, p_\kappa) &= p_\kappa h_\kappa^{-d} \sum_{F \in \mathcal{F}_{\mathtt{CFE}}} C_m(p_\kappa, \kappa, F)\sigma^{-1}|F| \\ &+ p_\kappa^2 |\kappa|^{-1} \sum_{F \in \mathcal{F}_{\mathtt{CFE}}} C_{\mathrm{INV}}(p_\kappa, \kappa, F)\sigma^{-1}|F| + h_\kappa^{-d+2} p_\kappa^{-1} \sum_{F \in \mathcal{F}_{\mathtt{CFE}}} C_m(p_\kappa, \kappa, F)\sigma|F|,\end{aligned}$$

with $s_\kappa = \min\{p_\kappa + 1, k_\kappa\}$ and $p_\kappa \geq 1$. Here, C is a positive constant which is independent of the discretization parameters.

Proof. See [21] for details. □

Remark 3.4. *For uniform orders $p_\kappa = p \geq 1$, $h = \max_{\kappa \in \mathcal{M}_{\mathtt{CFE}}} h_\kappa$, $s_\kappa = s$, $s = \min\{p + 1, k\}$, $k > 1 + d/2$, under the assumption that the diameter of the faces of each element $\kappa \in \mathcal{M}_{\mathtt{CFE}}$ is of comparable size to the diameter of the corresponding element, the* a priori *error bound stated in Theorem 3.2 coincides with the bounds derived in [35, 41], for example, for DGFEMs defined on standard element domains. In particular, this bound is optimal in h and suboptimal in p by $p^{1/2}$.*

4 Hyperbolic PDEs

In this section we consider the generalization of CFE/DGFEMs posed on general polytopic meshes for the numerical approximation of first–order hyperbolic PDEs. To this end, we consider the following model problem: find u such that

$$\begin{aligned}\nabla \cdot (\mathbf{b}u) + cu &= f \quad \text{in } \Omega, &(10)\\ u &= g \quad \text{on } \partial_-\Omega, &(11)\end{aligned}$$

where $c \in L_\infty(\Omega)$, $f \in L_2(\Omega)$, and $\mathbf{b} = (b_1, b_2, \ldots, b_d)^\top \in [W^1_\infty(\Omega)]^d$. Here, the inflow and outflow portions of the boundary $\partial\Omega$ are defined, respectively, by

$$\partial_-\Omega = \Big\{\mathbf{x} \in \partial\Omega : \mathbf{b}(\mathbf{x}) \cdot \mathbf{n}(\mathbf{x}) < 0\Big\}, \quad \partial_+\Omega = \Big\{\mathbf{x} \in \partial\Omega : \mathbf{b}(\mathbf{x}) \cdot \mathbf{n}(\mathbf{x}) \geq 0\Big\},$$

where $\mathbf{n}$ denotes the unit outward normal vector to the boundary $\partial\Omega$. Throughout this section, we assume that the following (standard) positivity condition holds: there exists a positive constant γ_0 such that

$$c_0(x)^2 = c(x) + \frac{1}{2}\nabla\cdot\mathbf{b}(x) \geq \gamma_0 \quad \text{a.e. } x \in \Omega. \tag{12}$$

The DGFEM approximation to (10)-(11) is then given by: find $u_h \in V(\mathcal{M}_{\mathtt{CFE}}, \boldsymbol{p})$ such that

$$B_{\mathtt{Hyp}}(u_h, v_h) = F_{\mathtt{Hyp}}(v_h) \tag{13}$$

for all $v_h \in V(\mathcal{M}_{\mathtt{CFE}}, \boldsymbol{p})$, where

$$\begin{aligned} B_{\mathtt{Hyp}}(w,v) &= \sum_{\kappa\in\mathcal{M}_{\mathtt{CFE}}} \left\{ \int_\kappa \Big(-w\mathbf{b}\cdot\nabla v + cwv \Big)\,\mathrm{d}\mathbf{x} + \int_{\partial\kappa} \mathcal{H}(w_\kappa^+, w_\kappa^-, \mathbf{n}_\kappa) v_\kappa^+ \,\mathrm{d}s \right\}, \\ F_{\mathtt{Hyp}}(v_h) &= \int_\Omega f v_h \,\mathrm{d}\mathbf{x}. \end{aligned}$$

Here, $\mathcal{H}(w_\kappa^+, w_\kappa^-, \mathbf{n}_\kappa)|_{\partial\kappa}$, which depends on both the inner– and outer–trace of w on $\partial\kappa$, $\kappa \in \mathcal{M}_{\mathtt{CFE}}$, and the unit outward normal vector $\mathbf{n}_\kappa$ to $\partial\kappa$, is a *numerical flux* function; this serves as an approximation to the normal flux $(\mathbf{b}u)\cdot\mathbf{n}_\kappa$ on the boundary of each element $\kappa \in \mathcal{M}_{\mathtt{CFE}}$. The numerical flux function $\mathcal{H}(\cdot,\cdot,\cdot)$ may be chosen to be any two-point monotone Lipschitz function which is both consistent and conservative; see [38, 46], for example. In the current setting, the most natural choice of numerical flux is the standard upwind flux given by

$$\mathcal{H}(u_h^+, u_h^-, \mathbf{n}_\kappa)|_F = \begin{cases} \mathbf{b}\cdot\mathbf{n}_\kappa \lim_{s\to 0^+} u_h(\mathbf{x} - s\mathbf{b}) & F \subset \partial\kappa\backslash\partial_-\Omega, \ \ \kappa \in \mathcal{M}_{\mathtt{CFE}}, \\ \mathbf{b}\cdot\mathbf{n}_\kappa\, g & F \subset \partial\kappa \cap \partial_-\Omega, \ \ \kappa \in \mathcal{M}_{\mathtt{CFE}}, \end{cases}$$

for all $F \in \mathcal{F}_{\mathtt{CFE}}$, cf. [26].

Using the above definition of the numerical flux function $\mathcal{H}(\cdot,\cdot,\cdot)$, the DGFEM (13) can be rewritten in the following equivalent form: find $u_h \in V(\mathcal{M}_{\mathtt{CFE}}, \boldsymbol{p})$ such that

$$\tilde{B}_{\mathtt{Hyp}}(u_h, v_h) = \tilde{F}_{\mathtt{Hyp}}(v_h)$$

for all $v_h \in V(\mathcal{M}_{\mathtt{CFE}}, \boldsymbol{p})$, where

$$\begin{aligned} \tilde{B}_{\mathtt{Hyp}}(w,v) &= \sum_{\kappa\in\mathcal{M}_{\mathtt{CFE}}} \int_\kappa \Big(-w\mathbf{b}\cdot\nabla v + cwv \Big)\,\mathrm{d}\mathbf{x} \\ &\quad + \sum_{\kappa\in\mathcal{M}_{\mathtt{CFE}}} \left\{ \int_{\partial_+\kappa} \mathbf{b}\cdot\mathbf{n}_\kappa\, w_\kappa^+ v_\kappa^+ \,\mathrm{d}s + \int_{\partial_-\kappa\backslash\partial_-\Omega} \mathbf{b}\cdot\mathbf{n}_\kappa\, w_\kappa^- v_\kappa^+ \,\mathrm{d}s \right\}, \\ \tilde{F}_{\mathtt{Hyp}}(v_h) &= \int_\Omega f v_h \,\mathrm{d}\mathbf{x} - \sum_{\kappa\in\mathcal{M}_{\mathtt{CFE}}} \int_{\partial_-\kappa\cap\partial_-\Omega} \mathbf{b}\cdot\mathbf{n}_\kappa\, g v_\kappa^+ \,\mathrm{d}s. \end{aligned}$$

Remark 4.1. *We note that, upon application of integration by parts elementwise, the bilinear form $\tilde{B}_{\mathtt{Hyp}}(\cdot,\cdot)$ may be written in the familiar form:*

$$\begin{aligned}\tilde{B}_{\mathtt{Hyp}}(w,v) &= \sum_{\kappa\in\mathcal{M}_{\mathtt{CFE}}}\int_\kappa \Big(\nabla\cdot(\mathbf{b}w)\,v + cwv\Big)\,\mathrm{d}\mathbf{x} \\ &\quad - \sum_{\kappa\in\mathcal{M}_{\mathtt{CFE}}}\left\{\int_{\partial_-\kappa\setminus\partial_-\Omega}\mathbf{b}\cdot\mathbf{n}_\kappa\,(w_\kappa^+ - w_\kappa^-)v_\kappa^+\,\mathrm{d}s + \int_{\partial_-\kappa\cap\partial_-\Omega}\mathbf{b}\cdot\mathbf{n}_\kappa\,w_\kappa^+v_\kappa^+\,\mathrm{d}s\right\},\end{aligned}$$

cf. [35, 20], for example.

4.1 Error analysis

The analysis of the DGFEM (13) in the *hp*–version setting may be tackled by a number of different approaches. In the articles [13, 34], additional streamline–diffusion terms are included within the underlying discretization method; in this setting, optimal *hp*–error bounds may then be derived in a straightforward manner. However, as noted in [34], the streamline–diffusion stabilization offers very little, if any, practical advantage over the standard DGFEM (with no stabilization), and is mainly employed for analysis purposes. In the absence of streamline–diffusion stabilization, under the assumption that

$$\mathbf{b}\cdot\nabla_h\xi \in V(\mathcal{M}_{\mathtt{CFE}},\boldsymbol{p}) \quad \forall\xi\in V(\mathcal{M}_{\mathtt{CFE}},\boldsymbol{p}), \tag{14}$$

holds, together *hp*–optimal approximation results for the local L_2–projector, optimal *hp*–bounds for (13) have been derived in the article [35] for meshes consisting of shape-regular d–parallelepipeds. For *hp*–optimal approximation results of the L_2–projector on d–simplices, we refer to [23].

Following [20], for the case when general polytopic elements are admitted, in the absence of optimal *hp*–approximation results for the local L_2–projection operator, we prove an inf-sup condition for the bilinear form $\tilde{B}_{\mathtt{Hyp}}(\cdot,\cdot)$, with respect to the following streamline DGFEM-norm:

$$|||v|||_{\mathrm{SD}}^2 = |||v|||_{\mathtt{Hyp}}^2 + \sum_{\kappa\in\mathcal{M}_{\mathtt{CFE}}}\tau_\kappa\|\mathbf{b}\cdot\nabla v\|_{L_2(\kappa)}^2, \tag{15}$$

where

$$|||v|||_{\mathtt{Hyp}}^2 = \sum_{\kappa\in\mathcal{M}_{\mathtt{CFE}}}\Big(\quad \|c_0v\|_{L_2(\kappa)}^2 + \frac{1}{2}\|v_\kappa^+\|_{\partial\kappa\cap\partial\Omega}^2 + \frac{1}{2}\|v_\kappa^+ - v_\kappa^-\|_{\partial_-\kappa\setminus\partial\Omega}^2\Big).$$

Here, c_0 is defined as in (12) and $\|\cdot\|_\tau$, $\tau\subset\partial\kappa$, denotes the (semi)norm associated with the (semi)inner product $(v,w)_\tau = \int_\tau|\mathbf{b}\cdot\mathbf{n}|vw\,\mathrm{d}s$. Finally, the streamline–diffusion parameter τ_κ, $\kappa\in\mathcal{M}_{\mathtt{CFE}}$, is given by

$$\tau_\kappa = \frac{1}{\|\mathbf{b}\|_{L_\infty(\kappa)}}\frac{1}{p_\kappa^2}\min_{F\subset\partial\kappa}\frac{\sup_{\kappa_\flat^F\subset\kappa}|\kappa_\flat^F|}{|F|}d \quad \forall\kappa\in\mathcal{M}_{\mathtt{CFE}}, \tag{16}$$

for $d = 2, 3$ and $p_\kappa \geq 1$, and $\kappa_\flat^F$ is as defined in Definition 3.2. In the case when $p_\kappa = 0$, τ_κ is formally defined to be zero.

Under the assumption that (14) holds, the following inf-sup condition for the bilinear form $\tilde{B}_{\mathtt{Hyp}}(\cdot,\cdot)$, with respect to the streamline DGFEM-norm (15), may be established, cf. [20]; this represents a generalization of the results in [15, 19].

Theorem 4.1. *Given Assumptions 3.1, 3.3, and 3.4 hold, there exists a positive constant Λ_s, independent of the mesh size h and the polynomial degree p, such that:*

$$\inf_{\nu \in V(\mathcal{M}_{\mathtt{CFE}},\boldsymbol{p})\setminus\{0\}} \sup_{\mu \in V(\mathcal{M}_{\mathtt{CFE}},\boldsymbol{p})\setminus\{0\}} \frac{\tilde{B}_{\mathtt{Hyp}}(\nu,\mu)}{|||\nu|||_{\mathrm{SD}}|||\mu|||_{\mathrm{SD}}} \geq \Lambda_s. \tag{17}$$

On the basis of the inf-sup condition stated in Theorem 4.1, together with the approximation results given in Lemma 3.3, we deduce the following *a priori* error bound for the DGFEM (13).

Theorem 4.2. *Let $\Omega \subset \mathbb{R}^d$, $d = 2, 3$, be a bounded polyhedral domain, and $\mathcal{M}_{\mathtt{CFE}} = \{\kappa\}$ be a subdivision of Ω consisting of general polytopic elements satisfying Assumptions 3.1, 3.3, and 3.4. Further, let $\mathcal{T}_\sharp = \{\mathcal{K}\}$ denote the associated covering of Ω consisting of shape-regular d–simplices as in Definition 3.1, which satisfies Assumption 3.2. Let $u_h \in V(\mathcal{M}_{\mathtt{CFE}}, \boldsymbol{p})$ be the DGFEM approximation to $u \in H^1(\Omega)$ defined by (13) and suppose that $u|_\kappa \in H^{k_\kappa}(\kappa)$, $k_\kappa > 1 + d/2$, for each $\kappa \in \mathcal{M}_{\mathtt{CFE}}$, such that $\mathcal{E}u|_{\mathcal{K}} \in H^{k_\kappa}(\mathcal{K})$, where $\mathcal{K} \in \mathcal{T}_\sharp$ with $\kappa \subset \mathcal{K}$. Then, the following error bound holds:*

$$|||u - u_h|||_{\mathrm{SD}}^2 \quad \leq \quad C \sum_{\kappa \in \mathcal{M}_{\mathtt{CFE}}} \frac{h_\kappa^{2s_\kappa}}{p_\kappa^{2k_\kappa}} \mathcal{G}_\kappa(F, C_m, p_\kappa, \tau_\kappa) \|\mathcal{E}u\|_{H^{k_\kappa}(\mathcal{K})}^2, \tag{18}$$

where

$$\begin{aligned} \mathcal{G}_\kappa(F, C_m, p_\kappa, \tau_\kappa) \quad &= \quad \|c_0\|_{L_\infty(\kappa)}^2 + \gamma_\kappa^2 + \tau_\kappa^{-1} + \tau_\kappa \beta_\kappa^2 p_\kappa^2 h_\kappa^{-2} \\ &\quad + \beta_\kappa p_\kappa h_\kappa^{-d} \sum_{F \subset \partial\kappa} C_m(p_\kappa, \kappa, F)|F|, \end{aligned} \tag{19}$$

$s_\kappa = \min\{p_\kappa + 1, k_\kappa\}$ and $p_\kappa \geq 1$. Here, $\gamma_\kappa = \|c_1\|_{L_\infty(\kappa)}$, with $c_1(x) = c(x)/c_0(x)$, c_0 as in (12), and $\beta_\kappa = \|\mathbf{b}\|_{L_\infty(\kappa)}$. The positive constant C is independent of the discretization parameters.

Remark 4.2. *For uniform orders $p_\kappa = p \geq 1$, $h = \max_{\kappa \in \mathcal{M}_{\mathtt{CFE}}} h_\kappa$, $s_\kappa = s$, $s = \min\{p + 1, k\}$, $k > 1 + d/2$, under the assumption that the diameter of the faces of each element $\kappa \in \mathcal{M}_{\mathtt{CFE}}$ is of comparable size to the diameter of the corresponding element, the error bound stated in Theorem 4.2 reduces to*

$$|||u - u_h|||_{\mathtt{Hyp}} \leq |||u - u_h|||_{\mathrm{SD}} \leq C \frac{h^{s-\frac{1}{2}}}{p^{k-1}} \|u\|_{H^k(\Omega)};$$

which is optimal in h and suboptimal in p by $p^{1/2}$. This generalizes the error estimate derived in [35] to general polytopic meshes under the same assumption (14).

Remark 4.3. *On the basis of the error analysis undertaken in both the current section and Section 3,* a priori *error bounds for the DGFEM discretization of second–order PDEs with non-negative characteristic form on general polytopic meshes may be established; for details, we refer to our recent article [20].*

5 Numerical experiments

In this section we present a series of computational examples to illustrate the performance of the DGFEM on general classes of polytopic meshes. The computational validation of the error bounds derived in Theorems 3.2 and 4.2 have been presented in [21] and [20], respectively; cf., also, [1]. Thereby, for the purposes of this section we consider the numerical approximation of incompressible flows in complicated geometries, cf. [30]. Throughout this section, we select $C_\sigma = 10$, cf. Lemma 3.4.

5.1 Example 1: Flow through a complicated T–pipe domain

In this first example we consider the application of goal–oriented dual–weighted–residual mesh adaptation for the DGFEM discretization of the incompressible Navier–Stokes equations, cf. [10]. To this end, the computational domain Ω is defined to be an upside–down T–shaped pipe, which has had a series of randomly located, randomly sized, holes removed from both the vertical and horizontal sections. Figure 3(a) depicts the initial composite mesh, constructed based on employing the algorithm outlined in Section 2, which consists of only 128 polygonal elements. Here, the inflow boundary is specified at the top of the vertical section of the pipe, i.e., along $y = 6$, $4 \leq x \leq 8$, where Poiseuille flow enters Ω; the left-hand and right-hand side boundaries of the horizontal portion of the pipe, located at $x = 0$, $0 \leq y \leq 3$ and $x = 12$, $0 \leq y \leq 3$, respectively, are defined to be outflow Neumann boundaries. No slip boundary conditions are imposed on the remaining walls of the T–pipe geometry, together with the boundaries of the circular holes; finally, we set $Re = 100$. This test case represents a modification of the test problem considered in [30].

Here we consider goal–oriented control of the error in the target functional J, defined by $J(\mathbf{u}, p) = p(10, 1.5) \approx 3.49924\text{E-}3$, where $\mathbf{u}$ and p denote the velocity and pressure of the underlying flow, respectively. More precisely, following the notation in [30], we may establish an (approximate) error representation formula of the form

$$J(\mathbf{u}, p) - J(\mathbf{u}_h, p_h) \approx \sum_{\kappa \in \mathcal{M}_{\mathrm{CFE}}} \eta_\kappa,$$

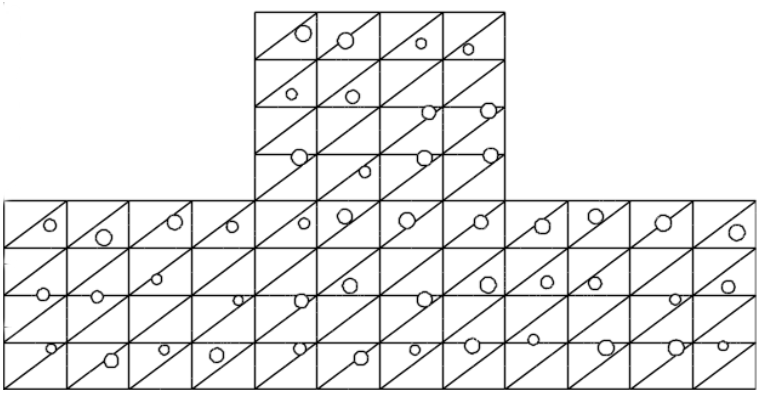

(a)

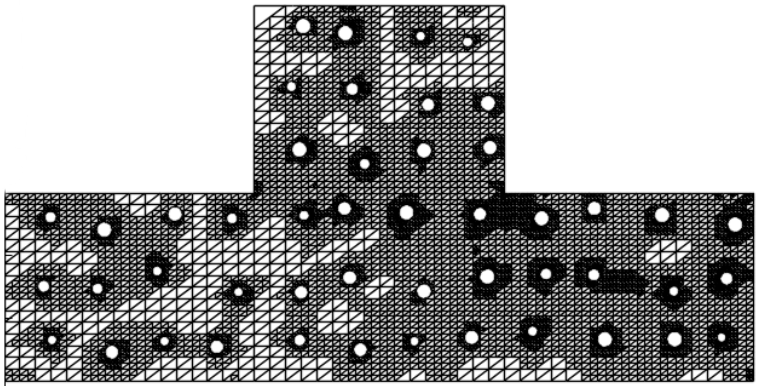

(b)

Figure 3: Example 1. (a) Initial composite finite element mesh consisting of 128 polygonal elements; (b) Composite mesh after 9 adaptive refinements with 13356 elements.

where $\mathbf{u}_h$ and p_h denote the DGFEM approximation to $\mathbf{u}$ and p, respectively, and η_κ, $\kappa \in \mathcal{M}_{\mathtt{CFE}}$, denote the corresponding (weighted) error indicators, which depend on both $\mathbf{u}_h$ and p_h, as well as the approximate solution of a corresponding dual problem; for full details, see [30].

In Table 1, we demonstrate the performance of exploiting an adaptive mesh refinement strategy based on marking elements for refinement according to the size of the local error indicators $|\eta_\kappa|$. Here, set the polynomial degrees for the approximation of the velocity field equal to 2, and employ piecewise discontinuous linear polynomials for the approximation of the pressure. In Table 1 we show the number of elements in the composite mesh $\mathcal{M}_{\mathtt{CFE}}$, the number of degrees of freedom in the underlying finite element space, the true error in the functional $J(\mathbf{u}, p) - J(\mathbf{u}_h, p_h)$, the computed error representation formula $\sum_{\kappa \in \mathcal{M}_{\mathtt{CFE}}} \eta_\kappa$, and the effectivity index $\theta = \sum_{\kappa \in \mathcal{M}_{\mathtt{CFE}}} \eta_\kappa / (J(\mathbf{u}, p) - J(\mathbf{u}_h, p_h))$. Here, we see that,

No of Eles	No of Dofs	$J(\mathbf{u},p)-J(\mathbf{u}_h,p_h)$	$\sum_{\kappa\in\mathcal{M}_{\mathtt{CFE}}}\eta_\kappa$	θ
128	1920	-2.207E-2	-1.583E-2	0.72
206	3090	-4.720E-3	-2.478E-3	0.52
356	5340	-3.720E-3	-1.909E-3	0.51
618	9270	-1.620E-3	-8.014E-4	0.49
1079	16185	-8.216E-4	-4.427E-4	0.54
1749	26235	-3.929E-4	-1.965E-4	0.50
2996	44940	-1.707E-4	-7.457E-5	0.44
4861	72915	-8.728E-5	-7.197E-5	0.82
8000	120000	-2.164E-5	-2.324E-5	1.07
13356	200340	-5.073E-6	-5.073E-5	1.00

Table 1: Example 1: Adaptive algorithm. We present the number of elements in the composite mesh $\mathcal{M}_{\mathtt{CFE}}$ and the corresponding number of degrees of freedom in $V(\mathcal{M}_{\mathtt{CFE}},\boldsymbol{p})$ (first two columns), the computed error in the target functional (third column), the sum of the (weighted) error indicators (fourth column), and the effectivity index (last column) at each step of the adaptive algorithm.

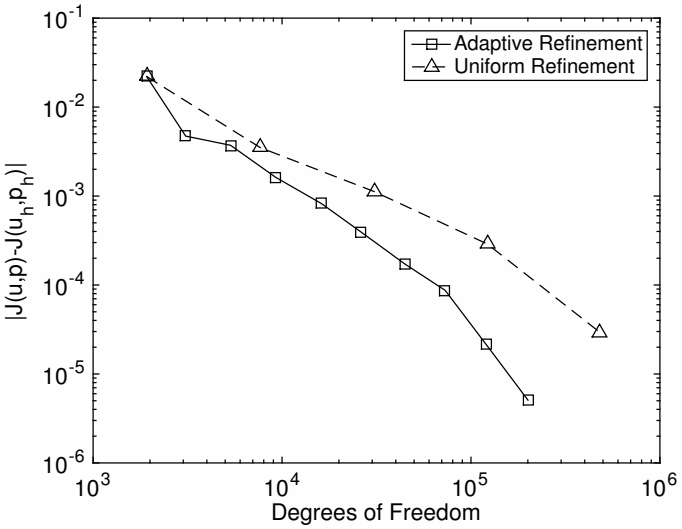

Figure 4: Example 1: Comparison between uniform and adaptive mesh refinement.

even on such coarse finite element meshes, the quality of the computed error representation formula is relatively good, in the sense that the effectivity indices are not too far away from unity. Indeed, as the mesh is refined, we observe that θ improves and approaches one. We note that *practical/engineering* accuracy can be attained using a very small number of degrees of freedom; indeed, fewer

degrees of freedom are necessary than what would be required to accurately mesh the domain Ω using standard element shapes. The results presented in Table 1 are plotted in Figure 4; here, we also compare the performance of the adaptive mesh refinement strategy with uniform mesh refinement. We observe that initially both strategies lead to a comparable error in the computed target functional of interest J, for a given number of degrees of freedom; however, as both refinement procedures continue, the adaptive algorithm leads to over an order of magnitude improvement in the error in J for a comparable number of degrees of freedom.

5.2 Example 2: Flow past a 3D scaffold geometry

In this final example, we consider incompressible flow past the three–dimensional scaffold geometry shown in Figure 1. More precisely, the domain Ω is defined to be the elliptical cylinder $\{(x,y) : (x-x_0)/a^2 + (y-y_0)^2/b^2 < 1\} \times (0.015, 1.14)$, with the scaffold removed; here $(x_0, y_0) = (4.1325, 4.1625)$, $a = 4.1175$, and $b = 4.1475$. Based on the work undertaken in the article [25], we model a Newtonian fluid with density $\rho = 1000kg/m^3$ and viscosity $\mu = 8.1 \times 10^{-4} Pa \cdot s$. Prescribing a flow rate of $53\mu ms^{-1}$ yields a Reynolds number, $Re = 2 \times 10^{-3}$. The fine mesh which accurately describes Ω is generated based on image data supplied by Prof. El Haj & Dr. Kuiper. Here, only a coarse model has been employed; a more detailed description of the scaffold geometry is presented in the articles [4, 5]. However, even for this 'coarse' model, the underlying fine finite element mesh consists of 15.8 million elements. To demonstrate the exploitation of general polytopic elements generated by agglomeration, we employ METIS [37] to generate a very coarse mesh consisting of only 32,000 elements. We prescribe an inlet Poiseuille flow on the top of the geometry, where $z = 1.14$, together with no-slip wall boundary conditions on both the outer vertical walls of the elliptical cylinder, as well as on the scaffold itself. The bottom portion of the geometry located at $z = 0.015$ is identified as an outflow Neumann boundary. In Figure 5 we plot the iso-surface of the magnitude of the velocity field; for the purposes of visualization, it was necessary to split the upper and lower regions of the computational domain. Clearly, by employing such a coarse agglomeration, we cannot expect that the computed DGFEM solution is sufficiently accurate, even within engineering constraints. However, this example clearly highlights a key issue we mentioned in Section 1: by employing polytopic elements, the dimension of the underlying finite element space is no longer proportional to the complexity of the geometry. Indeed, by exploiting *a posteriori* error estimation, cf. Example 1 above, then agglomerated elements may be marked for refinement; these can then be refined by again employing graph partitioning algorithms to the set of fine elements which form each marked (agglomerated) element. In this way, adaptive refinement of agglomerated elements, without the need to store mesh refinement trees, may be undertaken in a relatively simple manner, in order to automatically design polytopic meshes to yield reliable error control in

quantities of interest. This will be investigated as part of our future programme of research.

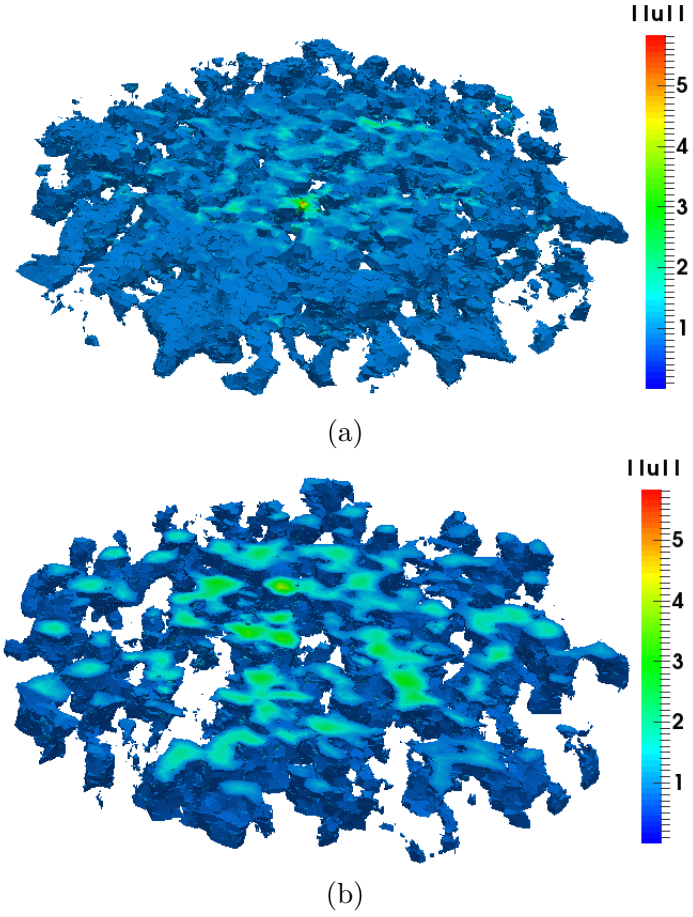

Figure 5: Example 2. Plot of the norm of the velocity field: (a) Upper section; (b) Lower section.

6 Concluding remarks

In this article, we have studied the application of DGFEMs on general finite element meshes consisting of polytopic elements. This class of methods is particularly attractive for a number of important reasons: (i) In the context of PDEs posed on complex domains Ω, the dimension of the underlying finite element space is independent of the number of small scale features/microstructures present in Ω; (ii) Adaptivity can easily be employed to enhance the error in the computed numerical solution by only refining regions of the domain which directly contribute to the error in given quantities of interest; (iii) High-order/hp–

finite elements are naturally admitted; (iv) The construction of coarse grid solvers for multilevel iterative solvers can easily be handled, cf. [2, 29]. In our present work, see, in particular, our recent articles [21, 20], great care has been taken to derive both inverse estimates and approximation results which are sharp with respect to element facet degeneration. This is particularly important for the definition of the interior penalty stabilization arising in the discretization of second–order elliptic PDEs. We believe this class of methods has huge potential for a wide variety of application areas, and in particular for problems arising in geophysics and biology. Indeed, as we have shown in Section 5, very complicated geometries can be treated, and with the use of general agglomerated refinement strategies, efficient and reliable computations may be undertaken. However, work on developing efficient quadrature and evaluation of appropriate stable polynomial bases on general polytopes still needs further work. Other future areas of research also include exploiting mesh partitioning algorithms for mesh refinement purposes, as well as the design and analysis of multilevel iterative solvers on polytopic meshes, for a wider range of application areas.

Acknowledgements

We would like to thank Prof. El Haj & Dr. Kuiper for supplying the data needed to generate the scaffold geometry shown in Figures 1 & 5.

References

[1] P.F. Antonietti, S. Giani, and P. Houston. *hp*–Version composite discontinuous Galerkin methods for elliptic problems on complicated domains. *SIAM J. Sci. Comput.*, 35(3):A1417–A1439, 2013.

[2] P.F. Antonietti, S. Giani, and P. Houston. Domain decomposition preconditioners for discontinuous Galerkin methods for elliptic problems on complicated domains. 60(1):203–227, 2014.

[3] P.F. Antonietti, P. Houston, M. Sarti, and M. Verani. Multigrid algorithms for *hp*–version interior penalty discontinuous Galerkin methods on polygonal and polyhedral meshes. *arXiv preprint arXiv:1412.0913*, 2014.

[4] E. Baas and J.H. Kuiper. A numerical model of heterogeneous surface strains in polymer scaffolds. *J. Biomech.*, 41:1374–1378, 2008.

[5] E. Baas, J.H. Kuiper, Y. Yang, M.A. Wood, and A.J. El Haj. In vitro bone growth responds to local mechanical strain in three-dimensional polymer scaffolds. *J. Biomech.*, 43:733–739, 2010.

[6] I. Babuška and J. E. Osborn. Generalized finite element methods: their performance and their relation to mixed methods. *SIAM J. Numer. Anal.*, 20(3):510–536, 1983.

[7] F. Bassi, L. Botti, and A. Colombo. Agglomeration-based physical frame dG discretizations: An attempt to be mesh free. *Math. Models Methods Appl. Sci.*, (8):1495–1539, 2014.

[8] F. Bassi, L. Botti, A. Colombo, D.A. Di Pietro, and P. Tesini. On the flexibility of agglomeration based physical space discontinuous Galerkin discretizations. *J. Comput. Phys.*, 231(1):45–65, 2012.

[9] F. Bassi, L. Botti, A. Colombo, and S. Rebay. Agglomeration based discontinuous Galerkin discretization of the Euler and Navier-Stokes equations. *Comput. & Fluids*, 61:77–85, 2012.

[10] R. Becker and R. Rannacher. An optimal control approach to a-posteriori error estimation in finite element methods. In A. Iserles, editor, *Acta Numerica*, pages 1–102. Cambridge University Press, 2001.

[11] L. Beirão da Veiga, F. Brezzi, A. Cangiani, G. Manzini, L.D. Marini, and A. Russo. Basic principles of virtual element methods. *Math. Models Methods Appl. Sci.*, 23(1):199–214, 2013.

[12] L. Beirão da Veiga, J. Droniou, and G. Manzini. A unified approach for handling convection terms in finite volumes and mimetic discretization methods for elliptic problems. *IMA J. Numer. Anal.*, 31(4):1357–1401, 2011.

[13] K.S. Bey and T. Oden. *hp*-Version discontinuous Galerkin methods for hyperbolic conservation laws. *Comput. Methods Appl. Mech. Engrg.*, 133:259–286, 1996.

[14] F. Brezzi, A. Buffa, and K. Lipnikov. Mimetic finite differences for elliptic problems. *M2AN Math. Model. Numer. Anal.*, 43(2):277–295, 2009.

[15] A Buffa, T.J.R. Hughes, and G Sangalli. Analysis of a multiscale discontinuous Galerkin method for convection-diffusion problems. *SIAM J. Numer. Anal.*, 44(4):1420–1440, 2006.

[16] E. Burman and P. Hansbo. Fictitious domain finite element methods using cut elements: I. A stabilized Lagrange multiplier method. *Comput. Methods Appl. Mech. Engrg.*, 199:2680–2686, 2010.

[17] E. Burman and P. Hansbo. An interior-penalty-stabilized Lagrange multiplier method for the finite-element solution of elliptic interface problems. *IMA J. Numer. Anal.*, 30:870–885, 2010.

[18] E. Burman and P. Hansbo. Fictitious domain finite element methods using cut elements: II. A stabilized Nitsche method. *Appl. Numer. Math.*, 62:328–341, 2012.

[19] A. Cangiani, J. Chapman, E.H. Georgoulis, and M. Jensen. On the stability of continuous–discontinuous Galerkin methods for advection–diffusion–reaction problems. *J. Sci. Comput.*, 57(2):313–330, 2013.

[20] A. Cangiani, Z. Dong, E.H. Georgoulis, and P. Houston. *hp*–Version discontinuous Galerkin methods for advection–diffusion–reaction problems on polytopic meshes. *Submitted for publication*, 2015.

[21] A. Cangiani, E.H. Georgoulis, and P. Houston. *hp*–Version discontinuous Galerkin methods on polygonal and polyhedral meshes. *Math. Models Methods Appl. Sci.*, 24(10):2009–2041, 2014.

[22] A. Cangiani, G. Manzini, and A. Russo. Convergence analysis of the mimetic finite difference method for elliptic problems. *SIAM J. Numer. Anal.*, 47(4):2612–2637, 2009.

[23] A. Chernov. Optimal convergence estimates for the trace of the polynomial L^2-projection operator on a simplex. *Math. Comp.*, 81(278):765–787, 2012.

[24] P.G. Ciarlet. *The finite element method for elliptic problems*. North-Holland Publishing Co., Amsterdam, 1978. Studies in Mathematics and its Applications, Vol. 4.

[25] M. Cioffi, F. Boschetti, M.T. Raimondi, and G. Dubini. Modeling evaluation of the fluid-dynamic microenvironment in tissue-engineered constructs: A micro-CT based model. *Biotech. Bioeng.*, 93(3):500–510, 2006.

[26] B. Cockburn, G.E. Karniadakis, and C.-W. Shu. The development of discontinuous Galerkin methods. In B. Cockburn, G.E. Karniadakis, and C.-W. Shu, editors, *Discontinuous Galerkin Methods: Theory, Computation and Applications*, volume 11 of *Lect. Notes Comput. Sci. Engrg.*, pages 3–50. Springer–Verlag, 2000.

[27] T.-P. Fries and T. Belytschko. The extended/generalized finite element method: an overview of the method and its applications. *Internat. J. Numer. Methods Engrg.*, 84(3):253–304, 2010.

[28] E.H. Georgoulis. Inverse-type estimates on *hp*-finite element spaces and applications. *Math. Comp.*, 77(261):201–219 (electronic), 2008.

[29] S. Giani and P. Houston. Domain decomposition preconditioners for discontinuous Galerkin discretizations of compressible fluid flows. *Numerical Mathematics: Theory, Methods & Applications*, 7(2), 2014.

[30] S. Giani and P. Houston. Goal-oriented adaptive composite discontinuous Galerkin methods for incompressible flows. *J. Comp. Appl. Math.*, 270:32–42, 2014.

[31] S. Giani and P. Houston. *hp*–Adaptive composite discontinuous Galerkin methods for elliptic problems on complicated domains. *Num. Meth. Part. Diff. Eqs.*, 30(4):1342–1367, 2014.

[32] W. Hackbusch and S.A. Sauter. Composite finite elements for problems containing small geometric details. Part II: Implementation and numerical results. *Comput. Visual Sci.*, 1:15–25, 1997.

[33] W. Hackbusch and S.A. Sauter. Composite finite elements for the approximation of PDEs on domains with complicated micro-structures. *Numer. Math.*, 75:447–472, 1997.

[34] P. Houston, C. Schwab, and E. Süli. Stabilized *hp*-finite element methods for first-order hyperbolic problems. *SIAM J. Numer. Anal.*, 37(5):1618–1643 (electronic), 2000.

[35] P. Houston, C. Schwab, and E. Süli. Discontinuous *hp*-finite element methods for advection-diffusion-reaction problems. *SIAM J. Numer. Anal.*, 39(6):2133–2163 (electronic), 2002.

[36] A. Johansson and M.G. Larson. A high order discontinuous Galerkin Nitsche method for elliptic problems with fictitious boundary. *Numer. Math.*, 123(4):607–628, 2013.

[37] G. Karypis and V. Kumar. A fast and highly quality multilevel scheme for partitioning irregular graphs. *SIAM J. Sci. Comput.*, 20(1):359–392, 1999.

[38] D. Kröner. *Numerical Schemes for Conservation Laws.* Wiley-Teubner, 1997.

[39] A. Massing. *Analysis and implementation of Finite Element Methods on overlapping and Fictitious Domains.* PhD thesis, University of Oslo, 2012.

[40] I. Perugia and D. Schötzau. An *hp*-analysis of the local discontinuous Galerkin method for diffusion problems. *J. Sci. Comput.*, 17(1-4):561–571, 2002.

[41] B. Rivière, M.F. Wheeler, and V. Girault. Improved energy estimates for interior penalty, constrained and discontinuous Galerkin methods for elliptic problems. I. *Comput. Geosci.*, 3(3-4):337–360 (2000), 1999.

[42] S. A. Sauter and R. Warnke. Extension operators and approximation on domains containing small geometric details. *East-West J. Numer. Math.*, 7(1):61–77, 1999.

[43] C. Schwab. *p– and hp–Finite element methods: Theory and applications in solid and fluid mechanics*. Oxford University Press: Numerical mathematics and scientific computation, 1998.

[44] E.M. Stein. *Singular Integrals and Differentiability Properties of Functions*. Princeton, University Press, Princeton, N.J., 1970.

[45] N. Sukumar and A. Tabarraei. Conforming polygonal finite elements. *Internat. J. Numer. Methods Engrg.*, 61(12):2045–2066, 2004.

[46] E. F. Toro. *Riemann Solvers and Numerical Methods for Fluid Dynamics*. Springer, 1997.

MOX Technical Reports, last issues

Dipartimento di Matematica
Politecnico di Milano, Via Bonardi 9 - 20133 Milano (Italy)

28/2015 Taffetani, M.; Ciarletta, P.
Beading instability in soft cylindrical gels with capillary energy: weakly non-linear analysis and numerical simulations

25/2015 Del Pra, M.; Fumagalli, A.; Scotti, A.
Well posedness of fully coupled fracture/bulk Darcy flow with XFEM

26/2015 Tagliabue, A.; Dede', L.; Quarteroni, A.
Nitsche's Method for Parabolic Partial Differential Equations with Mixed Time Varying Boundary Conditions

27/2015 Marron, J.S.; Ramsay, J.O.; Sangalli, L.M.; Srivastava, A.
Functional Data Analysis of Amplitude and Phase Variation

24/2015 Bonaventura, L:
Local Exponential Methods: a domain decomposition approach to exponential time integration of PDE.

23/2015 Paolucci, R.; Mazzieri, I.; Smerzini, C.
Anatomy of strong ground motion: near-source records and 3D physics-based numerical simulations of the Mw 6.0 May 29 2012 Po Plain earthquake, Italy

22/2015 Bonaventura, L.; Ferretti, R.
Flux form Semi-Lagrangian methods for parabolic problems

21/2015 Arena, M.; Azzone, G.; Secchi, P.; Vantini, S.
Reputational risk and corporate finance: A multi-event model

20/2015 Antonietti, P.F.; Formaggia, L.; Scotti, A.; Verani, M.; Verzotti, N.
Mimetic finite difference approximation of flows in fractured porous media

19/2015 Palamara, S.; Lange, M.; Vergara, C.; Lassila, T.; Frangi, A.F.; Quarteroni, A.
A coupled 3D-1D numerical monodomain solver for cardiac electrical activation in the myocardium with detailed Purkinje network